

1 **PacC-dependent adaptation and modulation of host cellular pH controls hemibiotrophic
2 invasive growth and disease development by the rice blast fungus**

3 Xiao-Lin Chen^{1,2,4}, Dan He¹, Changfa Yin¹, Jun Yang¹, Jing Sun¹, Dawei Wang¹, Minfeng Xue¹,
4 Zhigang Li¹, Zhao Peng¹, Deng Chen¹, Wensheng Zhao¹, Jin-Rong Xu³, Nicholas J. Talbot^{4*}, and
5 You-Liang Peng^{1*}

6

7 ¹State Key Laboratory of Agrobiotechnology and MOA Key Laboratory of the Monitoring and
8 Green Managements of Crop Pests, China Agricultural University, Beijing, China; ²State Key
9 Laboratory of Agricultural Microbiology and Provincial Key Lab of Plant Pathology of Hubei
10 Province, College of Plant Science and Technology, Huazhong Agricultural University, Wuhan,
11 China; ³Department of Botany and Plant Pathology, Purdue University, West Lafayette, USA; ⁴The
12 Sainsbury Laboratory, University of East Anglia, Norwich Research Park, Norwich, UK.

13

14 **Correspondence:**

15 *You-Liang Peng (email: pengyl@cau.edu.cn), *Nicholas J. Talbot (email: nick.talbot@tsl.ac.uk)

16 **Abstract**

17 Many of the world's most serious crop diseases are caused by hemibiotrophic fungi. These
18 pathogens have evolved the ability to colonize living plant cells, suppressing plant immunity
19 responses, before switching to necrotrophic growth, in which host cells die, providing the energy to
20 fuel sporulation and spread of the fungus. How hemibiotrophic pathogens switch between these two
21 lifestyles remains poorly understood. Here, we report that the devastating rice blast fungus,
22 *Magnaporthe oryzae*, manipulates host cellular pH to regulate hemibiotrophy. During infection by
23 *M. oryzae*, host plant cells are alkalinized to pH 7.8 during biotrophic growth, but later acidified to
24 pH 6.5 during necrotrophy. Using a forward genetic screen, we identified alkaline-sensitive mutants
25 of *M. oryzae* that were blocked in biotrophic proliferation and impaired in induction of host cell
26 acidification and necrotrophy. These mutants defined components of the PacC-dependent ambient
27 pH signal transduction pathway in *M. oryzae*. We report that PacC exists as a full-length repressor,
28 PacC⁵⁵⁹, and a truncated transcriptional activator, PacC²²², which localize to the fungal nucleus
29 during biotrophic growth and to the cytoplasm during necrotrophy. During biotrophy, PacC²²²
30 directly activates genes associated with nutrient acquisition and fungal virulence, while PacC⁵⁵⁹
31 represses genes associated with saprophytic mycelial growth and sporulation, which are subsequently
32 de-repressed during necrotrophy. When considered together, our results indicate that temporal
33 regulation of hemibiotrophy by *M. oryzae* requires PacC-dependent sensing and manipulation of host
34 cellular pH.

35 **Author Summary**

36 Crop diseases caused by fungi represent some of the most serious threats to global food security.
37 Many fungal pathogens have evolved the ability to invade living plant tissue and suppress host
38 immunity, before switching to a completely different mode of growth, in which they are able to kill
39 host plant cells. This lifestyle— called hemibiotrophy —is exemplified by the blast fungus,
40 *Magnaporthe oryzae*, which causes devastating diseases of rice, wheat and many other grasses. We
41 found that during infection by *M. oryzae*, host cells initially have an alkaline pH, when the fungus is
42 growing in living tissue, but pH rapidly becomes acidic, as host tissue is killed. We identified
43 mutants of the blast fungus that were sensitive to alkaline pH and this enabled us to identify the
44 signal transduction pathway by which the fungus responds to changes in ambient pH. We found that
45 mutants in the pH response pathway were blocked in invasive fungal growth and could not cause
46 acidification of host tissue. Consequently, they are unable to cause blast disease. We characterized
47 the central regulator of this pathway, the PacC transcription factor, which unusually can act as both a
48 repressor and an activator of fungal gene expression. During biotrophic invasive growth, PacC
49 activates many genes previously reported to be required for virulence, including several associated
50 with nutrient acquisition, and at the same time represses genes associated with vegetative growth and
51 sporulation. The PacC signaling pathway is therefore necessary for regulating the switch in fungal
52 lifestyle associated with causing blast disease.

53 **Introduction**

54 Plant pathogenic fungi can be broadly classified into species that always invade living host tissue,
55 called biotrophs, which evade recognition and suppress host immunity to systemically colonize host
56 plants, and necrotrophic pathogens which overwhelm plant defenses by rapidly killing plant cells, to
57 acquire nutrients from dead or dying tissue [1-3]. Both groups of pathogens exhibit distinct
58 characteristics in terms of the weapons they deploy to infect host plants— such as effector proteins,
59 toxins, and metabolites [4]. Host plants have, in turn, evolved distinct immune signaling pathways to
60 respond to biotrophs and necrotrophs [5]. There is, however, a third group of pathogens,
61 encompassing many of the world's most serious disease-causing fungi that exhibit both styles of
62 growth. These pathogens are known as hemibiotrophs and initially infect plants like a biotroph,
63 eliciting little response or disease symptoms in their host, but later, at a given point during infection,
64 they switch to killing cells, inducing cellular necrosis and fueling their own sporulation [1]. However,
65 the mechanism by which hemibiotrophic fungal pathogens switch between biotrophy and
66 necrotrophy remains poorly understood [4,6].

67 Rice blast disease is one of the most devastating diseases threatening rice production worldwide
68 [7-8], and is caused by *Magnaporthe oryzae* (syn. *Pyricularia oryzae*), a hemibiotrophic fungus
69 [6,9-10]. The fungus initiates infection by forming a specialized infection cell called an appressorium
70 which ruptures the host cuticle allowing invasive hyphae to enter rice cells (IH) [8,10]. These
71 biotrophic IH are surrounded by a host-derived extra-invasive hyphal membrane (EIHM) [9], and
72 contribute to secretion of apoplastic and cytoplasmic effectors [8,11]. Apoplastic effectors are often
73 N-glycosylated and secreted via the conventional endoplasmic reticulum-Golgi secretion pathway
74 [11-14]. They fulfill diverse roles, including suppression of chitin-triggered immunity [13-14]. By
75 contrast, cytoplasmic effectors are secreted via a plant membrane-derived biotrophic interfacial
76 complex (BIC), using a Golgi-independent process [8,11-12]. These effectors enable *M. oryzae* to
77 grow in epidermal tissue and move from cell to cell using pit field sites [15]. A fungal nitronate

78 monooxygenase, Nmo2, involved in the nitrooxidative stress response, is also required to avoid
79 triggering plant immunity, thereby facilitating growth and BIC development of *M. oryzae* [16]. Host
80 cells begin to lose viability, once invasive hyphae begin to invade adjacent cells and the switch to
81 necrotrophic growth. This accompanies the appearance of necrotic disease lesions, from which the
82 fungus sporulates [10].

83 In this study, we set out to explore the mechanism by which *M. oryzae* switches from biotrophic
84 to necrotrophic growth. Specifically, we decided to test the hypothesis that modulation of host
85 cellular pH may be involved in the regulation of this morphogenetic and physiological switch [17].
86 Alkalization of plant cells is an important early immune response to attack by pathogens [18-21],
87 and some pathogens have developed mechanisms to alter pH of plant tissues [17,22]. The
88 necrotrophic pathogens *Athelia rolfsii* and *Sclerotinia sclerotiorum* both, for instance, generate
89 oxalic acid, leading to a sharp drop in the pH of host cells [23-24], while *Fusarium oxysporum*
90 secretes a rapid alkalization factor to induce host tissue alkalization [25].

91 Fungi are generally more acidophilic and have evolved array of mechanisms to adapt to ambient
92 alkaline pH, including the well-known PacC signaling pathway [26]. In *Aspergillus nidulans*, the
93 PacC-dependent pH signaling pathway consists of eight proteins, PacC, PalA, PalB, PalC, PalF,
94 PalH, PalI, and Vps32 [26-27]. The PalH protein is a transmembrane domain-containing protein and
95 functions as an alkaline pH sensor by interacting with an arrestin-like protein, PalF, through its
96 C-terminal domain [28-30]. PalI is also a plasma membrane protein which assists in the localization
97 of PalH [28]. Under alkaline pH conditions, PalF is phosphorylated and ubiquitinated to transduce
98 upstream pH signals [29]. The PalC protein binds to Vps32 by its Bro1-like domain and is a potential
99 linker between the plasma membrane and the endosomal complex [27]. The endosomal protein
100 Vps32 can combine with ESCRT-III (the Endosomal Sorting Complex Required for Transport III)
101 and functions in cargo sorting in the Multi-Vesicular Body (MVB) [31]. The calpain-like protease
102 PalB then assembles Vps32 and PalA as a complex to proteolytically process the transcription factor

103 pacC [32-33].

104 Under acidic conditions, *A. nidulans* full-length PacC predominantly exists in a
105 protease-inaccessible closed conformation within the cytoplasm. In this conformation, region A
106 (169-301 aa) and region B (334-410 aa) of PacC together interact with the negatively-acting
107 C-terminal domain C (529-678 aa), resulting in a closed conformation [34]. Under alkaline
108 conditions, the interaction is disrupted by upstream Pal proteins and PacC then forms a
109 protease-accessible ‘open conformation’, from which the negatively acting C-terminal domain is
110 removed by two protease cleavage steps. First, the full-length 674-residue pacC72 is cleaved into an
111 intermediate form, pacC53, by removal of the 180 amino acid residues of the C-terminus [35]. In this
112 process, PalA is bound to two YPXL/I motifs beside the 24-residue highly conserved signaling
113 protease box in the C-terminus of PacC, and PalB is likely to be the protease that catalyzes the
114 cleavage [36]. The intermediate pacC53 is then further processed by removal of an additional 245
115 amino acid residues from the C-terminus to yield a 250-residue form pacC27 [35,37]. The functional
116 pacC27 contains three Cys2His2 zinc fingers (ZF) and binds to the *cis*-element GCCARG through
117 ZF2 and ZF3 [38-39]. The GCCARG consensus exists in the promoters of genes expressed
118 preferentially under conditions of alkaline ambient pH and also genes repressed at alkaline ambient
119 pH, but expressed preferentially at acidic ambient pH [38]. Although the PacC orthologues in
120 *Saccharomyces cerevisiae* and *Candida albicans* bind to similar *cis*-elements in the promoters of the
121 regulated genes and are dependent on palB for proteolytical processing, their resulting forms and
122 function are distinct from PacC in *A. nidulans*. In *S. cerevisiae*, the PacC counterpart Rim101p is
123 processed by a single step and functions mainly as a transcriptional repressor [40-41]. In *C. albicans*,
124 CaRim101p is an 85kDa protein with a 74-kDa form in alkaline pH and a 65-kDa form at acidic pH,
125 respectively [42]. CaRim101p can also function as both an activator and a repressor. For example, it
126 can directly activate PHR1 (the alkaline-expressed gene) and repress PHR2 (the acidic-expressed
127 gene) [43-44]. However, how fungal PacC proteins function as both transcriptional activators and

128 repressors is still relatively poorly understood.

129 Here, we show that upon infection by *M. oryzae*, host plant cells are alkalinized to pH 7.8 during
130 the biotrophic growth stage, but then acidified to pH 6.5 at the onset of necrotrophic growth. We
131 report that fungal adaptation to host alkalinization and the induction of host acidification requires the
132 PacC pH signaling pathway. We used a forward genetic screen to identify mutants that were
133 sensitive to alkaline pH, and found that they were all impaired in virulence. We went on to
134 characterise the PacC signaling pathway in the rice blast fungus. We show that in *M. oryzae* the
135 PacC transcription factor simultaneously exists as both a truncated transcriptional activator and a
136 full-length transcriptional repressor, that both localize to the nucleus during biotrophic growth of *M.*
137 *oryzae*. PacC acts as a key transcriptional regulator which coordinates expression of more than 25%
138 of the protein-encoding genes in *M. oryzae* to facilitate the hemibiotrophic switch, which is
139 necessary for rice blast disease. Plant cellular pH is therefore likely to be a key regulatory signal, that
140 is perceived and modulated by *M. oryzae* to control hemibiotrophic growth.

141

142 **Results**

143 **Host plant cells are alkalinized during biotrophic growth but acidified during necrotrophic 144 growth of *M. oryzae***

145 To investigate the effect of *M. oryzae* infection on host cellular pH, we first established a calibration
146 curve (S1A Fig) to measure cellular pH in barley leaf epidermis using the ratiometric
147 fluorescein-based pH sensitive dye method [45]. Using this method, we observed that pH in the
148 initially infected barley epidermal cells was elevated from pH6.8 to pH7.2 at 12 hours post
149 inoculation (hpi) as appressoria penetrated epidermal cells, and peaked at pH7.8 at 18 hpi when
150 primary infection hyphae had differentiated into bulbous invasive hyphae (IH). However, a decrease
151 to pH7.3 then occurred by 30 hpi as IH rapidly occupied host cells, and then to pH6.5 after 36 hpi
152 when the entire epidermal cell was filled with IH (Fig 1A-1B; S1B Fig). We also measured pH in

153 neighboring plant cells. To our surprise, these uninfected plant cells also became alkalinized by 12
154 hpi, reaching pH 7.8 by 24 hpi but then became acidic once occupied by *M. oryzae* IH at 48 hpi (Fig
155 1A-1B). These results show that the pH of host cells is significantly alkalinized during initial
156 infection, but acidified once IH proliferate in host tissue.

157 We then investigated the living viability of infected host cells with Trypan Blue, which
158 selectively stains dead cells [46], and observed that the first infected plant cells at most infection
159 sites only become stained by the Trypan Blue after 36 hpi, (Fig. 1D and E), indicating that initially
160 infected cells are alive before 30 hpi, but lose viability thereafter. Similarly, secondary infected plant
161 cells at most infection sites lost viability after 42 hpi but not before (Fig 1D-1E). Taken together, we
162 reason that host cellular alkalinization occurs during biotrophic growth, probably as an immune
163 response, whereas cellular acidification is associated with the induction of host cell death by *M.*
164 *oryzae* as the fungus switches to necrotrophic growth.

165 To understand the physiological consequences of the changes in pH during plant infection, we
166 assayed colony growth and conidiation of *M. oryzae* under different pH. In all three different *M.*
167 *oryzae* strains assayed, an alkaline of pH 7.8 was inhibitory whereas the acidic pH 6.5 was favorable
168 to both fungal growth and conidiation (Fig 1F; S2 Fig).

169

170 **Alkaline-sensitive mutants of *M. oryzae* are impaired in plant infection**

171 To understand the mechanism by which *M. oryzae* adapts to the alkalinized pH of plant cells, we
172 screened a T-DNA insertion mutant library of *M. oryzae* for mutants that were sensitive to pH 7.7
173 and identified nine mutants (S3A Fig) [47]. The mutants showed reduced colony growth, conidiation
174 and virulence (S3A-3C Fig). Co-segregation analyses indicated that sensitivity to the alkaline pH
175 was caused by the T-DNA insertion (S1 Table). To identify the genes disrupted in these nine
176 mutants, sequences flanking the T-DNA insertion sites were obtained by TAIL-PCR [48]. In mutants
177 CD3179, CD5893, CD9848, and XXY8938, the T-DNA was inserted in promoters or coding regions

178 of *MGG_01615*, *MGG_06335*, *MGG_06440*, and *MGG_09311*, respectively. In the remaining
179 mutants, T-DNA was inserted in the promoter or coding region of the same gene *MGG_10150* (S3D
180 Fig). Strikingly, *MGG_01615*, *MGG_06335*, *MGG_06440*, *MGG_09311* and *MGG_10150* are
181 orthologues of *palF*, *palB*, *palH*, *palC* and *pacC* in the PacC-pH signaling pathway in *A. nidulans*
182 [49], and were therefore named *PalF*, *PalB*, *PalH*, *PalC*, and *PacC*, respectively, in this study.
183 Among them, *PacC* encodes the central zinc-finger transcriptional regulator of the pathway.

184 To confirm mutant phenotypes, targeted gene deletion mutants were generated for *PalF*, *PalB*,
185 *PalH*, *PalC*, and *PacC* (S4A-4E Fig). All the resulting deletion mutants were sensitive to pH 7.7 and
186 formed darker colonies with reduced growth rates (Fig 2A; S2 Table). In addition, these mutants
187 were reduced in conidiation by 80-90%; compared to the isogenic wild type strain (Fig 2B). In
188 infection assays with barley and rice seedlings, mutants formed tiny lesions mixed with a few larger
189 yellow spots. Under the same conditions, the wild type strain produced numerous larger typical blast
190 disease lesions (Fig 2C). Re-introduction of the corresponding wild-type allele into each null mutant
191 rescued all defects, including sensitivity to alkaline pH. Therefore, disruption of the PacC pH
192 signaling pathway genes makes *M. oryzae* sensitive to alkaline pH and results in a reduction in
193 virulence.

194 In *A. nidulans*, *PalI*, *PalA* and *Vps32* are also involved in the PacC-pH signaling pathway [48].
195 However, *M. oryzae* mutants disrupted in these three genes were not identified in our screen. We
196 therefore generated Δ *palI* (*MGG_02630*), Δ *palA* (*MGG_00833*) and Δ *vps32* mutants (S4F-4H Fig).
197 To our surprise, these mutants displayed similar phenotypes to the wild type, including pH sensitivity
198 conidiation and virulence (Fig 2A-2C). Therefore, *PalA*, *PalI* and *Vps32* are dispensable for
199 regulating the alkaline pH response and virulence, suggesting that these three genes are not required
200 in the PacC signaling pathway of *M. oryzae*, at least during plant infection.

201

202 **PacC pathway mutants are impaired in biotrophic growth, induction of host cell acidification**

203 **and the switch to necrotrophy**

204 To understand why PacC pathway mutants are reduced in virulence, we compared their ability to
205 infect host cells with that of the wild type *M. oryzae* strain P131. During infection of barley leaf
206 epidermis, $\Delta palF$, $\Delta palB$, $\Delta palH$, $\Delta palC$ and $\Delta pacC$ mutants showed similar penetration frequencies
207 to the isogenic wild type, but were retarded at the stage of primary infection hyphal growth in more
208 than 70% of infection sites at 24 hpi. Under the same conditions, the P131 developed branched IH at
209 more than 70% of infection sites and by 30 hpi, it had formed branched IH in nearly 90% of infection
210 sites, with invasive hyphae spreading into neighboring plant cells at some infection sites. By
211 contrast, only 10% of appressoria formed branched IH in PacC pathway mutants (Fig 2D-2E).
212 However, $\Delta palI$, $\Delta palA$ and $\Delta vps32$ mutants were similar to the wild type P131 in development of
213 IH. These data indicate that *M. oryzae* has a PacC pathway that is crucial for biotrophic growth.

214 To investigate whether subsequent stages of infection are affected by loss of PacC signaling,
215 we inoculated wounded rice leaves to circumvent the need for appressorium-mediated penetration.
216 The wild type P131 generated large lesions, while PacC pathway mutants, including $\Delta pacC$, formed
217 significantly smaller lesions without evident necrosis (Fig 2F). We stained $\Delta pacC$ -infected barley
218 leaves with Trypan blue, and observed that the $\Delta pacC$ mutant led to host cell death at a much
219 delayed time (Fig 1E), suggesting that the mutant is deficient both in its ability to undertake
220 biotrophic growth and its switch to necrotrophy. In addition, the $\Delta pacC$ mutant induced less reactive
221 oxygen species (ROS) generation in host cells. However, inhibition of ROS production by
222 diphenyleneiodonium (DPI) treatment failed to allow IH to recover growth (Fig 2G), suggesting that
223 the reduced IH growth of PacC pathway mutants is due to factors other than ROS production.

224 We also monitored pH changes in barley cells infected by the $\Delta pacC$ mutant and observed that
225 pH in the initial host cells became alkalinized at 12 hpi, and then peaked at 7.8 at 24 hpi for the
226 initially colonized plant cells and at 36 hpi for the secondary infected cells, respectively (Fig 1B).
227 However, acidification of host cells infected by the $\Delta pacC$ mutant was much delayed (Fig 1B-1C).

228 These results indicate that the PacC pathway is necessary for inducing host cellular acidification but
229 not for host cellular alkalinization.

230

231 **PacC localizes to the fungal nucleus during biotrophic growth and under alkaline ambient pH**

232 To understand how the PacC pathway regulates biotrophic IH growth, we investigated the
233 subcellular localization of the PacC transcription factor during plant infection. We first generated an
234 *eGFP-PacC* fusion construct under control of the native *PacC* promoter and transformed it into a
235 $\Delta pacC$ mutant (Fig 5B). Subsequent phenotypic assays showed that all the resulting transformants
236 were recovered in colony growth, conidiation and virulence (Fig 5G-5H), indicating that the
237 GFP-fused PacC is functional. Interestingly, GFP signals were predominantly localized to the
238 nucleus in primary and branched IH from 18 to 30 hpi, but were then mainly distributed in the
239 cytoplasm from 36 hpi onwards (Fig 3A). Furthermore, GFP signals reappeared in the nuclei of IH
240 that had penetrated neighboring cells between 36 and 42 hpi, and then disappeared again from the
241 nucleus at 48 hpi (Fig 3A). By contrast, in pre-penetration stage structures, conidia and appressoria,
242 GFP signals were evenly distributed in the cytoplasm (Fig 3A). These data reveal that PacC localizes
243 to the nucleus specifically during biotrophic invasive growth.

244 Because host cells are alkalinized and acidified during biotrophic and necrotrophic growth,
245 respectively, we suspected that host cellular pH was the inductive signal for PacC nuclear
246 localization. To test this idea, we investigated the subcellular localization of PacC in mycelium
247 cultured under different pH. When the $\Delta pacC/GFP-PacC$ strain was cultured in liquid CM with pH
248 < 7.2 , GFP-PacC fluorescence was mainly observed in the cytoplasm (Fig 3B-3C). By contrast,
249 when hyphae were cultured at pH ≥ 7.2 , a proportion of the GFP signal localized to the nucleus; in
250 particular, the majority of the GFP signals localized to the nucleus at pH 7.7, as observed in the
251 branched IH. These observations indicate that alkaline pH is an important signal to induce nuclear
252 localization of PacC, as previously reported in *A. nidulans* [37,39].

253 We also introduced the *eGFP-PacC* construct independently into the *ΔpalH*, *ΔpalF*, *ΔpalC* and
254 *ΔpalB* mutants, and examined GFP subcellular localization. GFP-PacC was evenly distributed in the
255 cytoplasm, but not in the nucleus of *ΔpalH*, *ΔpalF*, *ΔpalC* and *ΔpalB* transformants (Fig 3D).
256 Therefore, the alkaline pH-induced nuclear localization of PacC requires *PalB*, *PalC*, *PalF* and
257 *PalH*.

258

259 **PacC is a central regulator of gene expression for biotrophic growth of *M. oryzae***

260 To identify PacC-regulated genes, we then carried out RNA-seq analysis of barley seedlings infected
261 with either the wild type or *ΔpacC* mutant at 18 hpi. The two strains expressed a total of 10303 genes
262 (≥ 2 FPKM), of which, 2747 genes were differentially expressed (S1 Dataset), including 1485 genes
263 that have one or multiple GCCAAG *cis*-elements [38] for PacC binding in their promoters (Fig 4A;
264 S1 Dataset) (arbitrarily defined as the 1.5 kb fragment upstream of the translation codon). Among
265 these, 1485 PacC-directly regulated genes, 924 and 561 were repressed or activated in the mutant,
266 respectively (S1 Dataset), suggesting that PacC acts as both a transcriptional activator and a
267 repressor. Interestingly, most of the down-regulated genes showed the highest expression in
268 biotrophic IH (Fig 4B; S2 dataset) whereas most of the 561 up-regulated genes showed the highest
269 expression in penetrating appressoria, as well as during conidiation, germinated conidia or/and
270 mycelium (Fig 4C; S3 dataset), suggesting that during biotrophic growth, PacC enhances
271 biotrophy-related genes and represses genes involved in appressorial penetration, conidiation, and
272 necrotrophic growth.

273 To define the gene repertoire directly regulated by PacC during biotrophic growth, we analyzed
274 predicted subcellular locations (<http://www.genscript.com/wolf-psort.html>), protein domains (Pfam,
275 <http://pfam.xfam.org/>), and gene ontology functions (GO, <http://www.geneontology.org/>) of their
276 encoded proteins. This analysis revealed that extracellular and membrane proteins were highly
277 enriched (Fig 4D; S4 Dataset). Among predicted extracellular proteins, 255 proteins have Pfam

278 and/or GO annotations, including 172 proteins that are putative polysaccharide hydrolases,
279 peptidases/proteases or lipases (Fig 4E; S4 Dataset). Notably, approximately half of the
280 polysaccharide hydrolases observed are likely to be involved in plant cell wall degradation (S5
281 Dataset) [50], and the rest may be involved in remodeling the fungal cell wall. In addition, 180 of the
282 predicted membrane proteins have Pfam and/or GO annotations, including 114 putative
283 membrane-associated transporters, which may function together with extracellular hydrolases to
284 acquire carbon and nitrogen sources for biotrophic growth of IH (Fig 4F; S4 Dataset). Furthermore,
285 among genes directly regulated by PacC, over 80 have been functionally characterized and have
286 roles in suppressing plant immunity, cell wall remodeling, nutrient utilization and metabolic
287 processes, including *ALG1*, *BAS4*, *BUF1*, *ECH1*, *GEL1*, *GLN1*, *HEX1*, *MET13*, *NMO2*, *NMR3*,
288 *PMC2*, *MoABC7*, *SDH1*, *MoAbfB*, *MoARG7*, *MoALR2*, *MoCDA1*, *MoCDA3*, *MoCDA4*, *MoIMD4*,
289 *MoLDB1*, and *MoMyo2* (S4 Dataset). When considered together, these data suggest that PacC
290 coordinates gene expression to facilitate biotrophic growth of the fungus and temporally regulates
291 the onset of necrotrophy.

292

293 **The PacC transcription factor exists both as a transcriptional activator and repressor**

294 To reveal how PacC simultaneously acts as both a transcriptional activator and a repressor, we
295 performed immunoblot analyses of the eGFP-PacC protein in mycelium of a $\Delta pacC/GFP-PacC$
296 strain. A full-length 87 kDa fusion protein was detected with an anti-GFP antibody, together with
297 two truncated forms of 52 kDa and 36 kDa. At pH ≤ 6.6 , all three forms were mainly present in the
298 cytoplasm and only trace amounts were observed in the nucleus. However, as pH increased to 7.7,
299 the majority of the three isoforms localized to the nucleus (Fig 5A). Full-length PacC has two
300 predicted proteolytic sites positioned at the 80th and 222th amino acid residue, respectively,
301 (<http://www.expasy.org/tools/peptidecutter/>) (Fig 5B; S3 Table) that may lead to the production of
302 36 kDa and 52 kDa eGFP-fused peptides. To investigate the functions of these predicted truncated

303 versions of PacC, two constructs, *eGFP-PacC⁹⁶* (artificial truncate at the 96th amino acid) and
304 *eGFP-PacC²⁴⁵* (artificial truncate at the 245th amino acid), were expressed under control of the native
305 PacC promoter in a $\Delta pacC$ mutant to create transformants NGP96 and NGP245. The NGP96
306 transformants expressed a 36 kDa protein with a protein >36kDa. In the NGP245 transformant, a 52
307 kDa protein, and a 36 kDa protein were detected together with a protein > 52kDa. These data
308 suggested that the 36 kDa and 52 kDa proteins may be generated from the full length eGFP-PacC⁵⁵⁹
309 by processing, probably at the 80th and 222th aa sites (Fig 5C), respectively.

310 To determine which PacC isoform is responsible for transcriptional activation or repression,
311 three constructs were created in which the binding domain (BD) of the Gal4 protein on pGBKT7 was
312 fused with the full-length PacC (*pBD-PacC⁵⁵⁹*), the truncated PacC²⁴⁵ (*pBD-PacC²⁴⁵*) and PacC⁹⁶
313 (*pBD-PacC⁹⁶*). Transformants expressing pBD-PacC⁵⁵⁹ or pBD-PacC⁹⁶ were prototrophic for Trp but
314 failed to grow on SD-Trp-His plates. In contrast, transformants of pBD-PacC²⁴⁵ grew well on the
315 plates with galactosidase activity (Fig 5D), suggesting that PacC²⁴⁵ can produce a protein with
316 transcription activation capability. We also expressed and purified GST fusion proteins of PacC⁵⁵⁹,
317 PacC²²² and PacC⁸⁰ and verified that GST-PacC⁵⁵⁹ and GST-PacC²²², but not GST-PacC⁸⁰ could bind
318 to the GCCAAG consensus sequence (Fig. 5E). These data suggest that PacC²²² functions as a
319 transcriptional activator, but PacC⁵⁵⁹ may act as a transcriptional suppressor, and PacC⁸⁰ by itself
320 probably does not act as a transcription factor.

321 To confirm the *in vivo* regulatory functions of PacC⁵⁵⁹ and PacC²²², 22 genes with the
322 PacC-binding GCCAAG consensus in their promoters were randomly selected for qRT-PCR analysis
323 with total RNA from the WT, the $\Delta pacC$, NGP245, and NGP559 strains. Based on their expression
324 patterns, these genes were classified into three types (Fig 6). There were six type I genes, which were
325 repressed under alkaline conditions in the WT and NGP559, but up-regulated in the $\Delta pacC$ mutant
326 and NGP245 (Fig 6A), indicating that they are repressed by PacC⁵⁵⁹. Fourteen type II genes were
327 up-regulated in the wild type, NGP245 and NGP559 strains, but significantly reduced in the $\Delta pacC$

328 mutant (Fig 6B), confirming that PacC²²² is a transcription activator. We further assayed the
329 phenotypes of NGP96, NGP245 and NGP559 strains. Sensitivity to alkaline pH, conidiation and
330 virulence were fully complemented in NGP559, but only partially so in NGP245. No obvious
331 difference was observed between the $\Delta pacC$ mutant and NGP96 (Fig 5F-5H). When considered
332 together, these results provide evidence that PacC²²² functions as a transcription activator, PacC⁵⁵⁹ as
333 a transcription repressor, and that both activities are necessary for the full biological function of
334 PacC during plant infection by *M. oryzae*.

335

336 **PacC orchestrates distinct developmental processes by regulating a broad repertoire of**
337 **transcription factor-encoding genes**

338 To understand how *PacC* in *M. oryzae* affects the observed phenotypes, we analyzed the downstream
339 hierarchy of transcriptional regulation. To do this, we selected several transcription factor-encoding
340 genes directly regulated by PacC for functional analysis.

341 *MGG_01779* is a PacC-regulated Type II gene probably encoding a novel C6 zinc DNA binding
342 domain protein (Fig 7), named *PAG1* (for PacC Activated Gene 1). Its promoter has two GCCAAG
343 sites bound by PacC (Fig 7B). The $\Delta pag1$ mutant showed no obvious defects in colony growth or
344 conidiation (Fig 7C and D, S4J Fig), but was significantly impaired in IH branching and in virulence
345 (Fig 7E). *PAG1* therefore functions downstream of PacC to regulate biotrophic growth of IH.

346 *MGG_13156* is a Type I gene (named *PRG1* for PacC Repressed Gene 1) with a GCCAAG site
347 in its promoter (S5B Fig). It appears to be expressed at higher levels under acidic rather than alkaline
348 conditions, and was up-regulated in the $\Delta pacC$ mutant (S5A Fig). We also generated two $\Delta prg1$
349 mutants, neither of which had obvious growth defects (S4I Fig). However, transformants showing
350 de-repression of *PRG1* by PacC, produced smaller colonies (S5C-S5G Fig). Thus, *PRG1* is indeed

351 negatively regulated by PacC during mycelial growth and infection.

352 *HTF1* is a homeobox gene required for conidiophore formation [51]. It was repressed in the WT,
353 but up-regulated in the $\Delta pacC$ mutant under alkaline pH conditions and during plant infection (S6A
354 Fig). Its promoter contains a GCCAAG site (S6B Fig). The *PIG1* TF controls mycelial melanin
355 biosynthesis [52] and was repressed by PacC⁵⁵⁹ under alkaline pH (S7A Fig). Its promoter also has a
356 GCCAAG site (S7B Fig), indicating that PacC represses expression of *PIG1* and thus the $\Delta pacC$
357 mutant formed darker colonies for excess melanization (Fig 2A).

358 Taken together, these results indicate that PacC may orchestrate distinct developmental
359 processes in *M. oryzae*, by directly regulating a wide range of transcription factors, thereby leading
360 to large-scale transcriptional changes which are essential for establishing blast disease.

361 **Discussion**

362 Many of the most important plant pathogenic fungi are hemibiotrophs which are able to switch from
363 biotrophic growth and necrotrophic growth during plant infection [1-3,9-10,]. Very little, however, is
364 known regarding how these fungi switch between the two growth habits and, indeed, which signals
365 from the plant elicit such a dramatic developmental and physiological change. In this study, we
366 identified host cellular pH as an inductive signal for the necrotrophic switch in *M. oryzae*.

367 We found that that host cells around infection sites are initially and temporally alkalinized to pH
368 7.8 during biotrophic growth, but acidification to pH 6.5 then follows during necrotrophic growth
369 (Figure 1A-1B and 1D-1E). This observation contrasts with a previous study which indicated that
370 host cells infected by *M. oryzae* remains alkaline for up to 60 hpi [51]. Our results also showed that
371 pH alkalinization is independent of *PacC* function (Fig 1B-1C and 1E) and is clearly inhibitory to
372 fungal growth and conidiation, based on *in vitro* studies (Fig 1F-1G), suggesting that host cellular
373 alkalinization is a plant immune response to *M. oryzae*, as previously reported in other disease
374 systems [18-21]. However, later acidification of plant tissue appears to be an active process,
375 manipulated by *M. oryzae*, because a Δ *pacC* mutant of the fungus is deficient in its induction (Fig
376 1B-1C). Moreover, acidified pH is conducive to fungal growth and conidiation in vitro (Fig 1F-1G).
377 Therefore, biotrophic growth may require a mechanism of fungal adaptation to host pH alkalinization
378 while necrotrophic growth is an active process by which the fungus prepares for future propagation.

379 Many previous studies have showed that the *PacC* transcription factor is important for virulence
380 of plant fungal pathogens [54-58], but our study, however, offers a potential mechanism which
381 indicates that the *PacC* pathway (including the *PacC* transcription factor) is involved in the
382 regulation of fungal hemibiotrophy. We have shown that the *PacC* pathway is required for *M. oryzae*
383 not only to adapt to the host cellular alkalinized pH for biotrophic growth, but also to induce pH
384 acidification, which allows necrotrophic growth (Fig 1; Fig 2). In particular, the regulation of
385 hemibiotrophy involves shuttling of the *PacC* transcription factor between the nucleus and the

386 cytoplasm, whereby PacC localizes to the nucleus during biotrophic growth and alkaline pH, but to
387 the cytoplasm during necrotrophic growth and acidic conditions (Fig 2; Fig 5A). Interestingly, palH
388 in *A. nidulans* mechanistically resembles mammalian GPCRs [59], and this study has revealed its
389 requirement for virulence of *M. oryzae* (Fig. 2A-2E). When considered together, PalH there may be a
390 candidate target for development of antifungal drugs.

391 This study also showed that *M. oryzae* differs from other fungi in the composition of the PacC
392 pathway, and in the proteolytic processing of the PacC transcription factor. In *A. nidulans*, palI
393 enhances the plasma membrane localization of palH [28], and palA and Vps32 form a complex with
394 palB for proteolytic processing of pacC [32-33]. However, *M. oryzae* mutants lacking the three
395 orthologous proteins are indistinguishable from the wild type strain in alkaline pH sensitivity, colony
396 growth, conidiation and virulence (Fig.2), indicating that they are not required for PacC pH-signaling
397 in *M. oryzae*. The PacC transcription factor in *M. oryzae* has two functional forms, a full-length
398 transcriptional repressor and a medium truncated form that acts as transcription activator, both of
399 which are required for its biological function (Fig 5 and Fig 6). To achieve their distinct
400 transcriptional functions, *M. oryzae* PacC forms translocate to the nucleus during biotrophic growth
401 (Fig 3A), likely as a consequence of alkaline pH (Fig 1A-1B; Fig 3B), as reported for nuclear
402 localization of pacC in *A. nidulans* [37]. However, the two different *M. oryzae* PacC forms exist
403 independently of alkaline pH (Fig 5A). Therefor the processing of PacC in *M. oryzae* is different
404 from that reported in other fungi. In *A. nidulans*, pacC remains in the cytoplasm in its full-length
405 closed conformation, which is protease-inaccessible under acidic conditions, but is processed into the
406 activator form under alkaline pH (34-35,49). Furthermore, in *C. albicans*, the full length 85kDa
407 CaRim101p is partially processed into a 74 kDa, under protein neutral pH, but into a 64kDa protein
408 in acidic pH [42]; In *S. cerevisiae*, the full length 98 kDa Rim101p is cleaved into an active 90kDa
409 form in alkaline pH [60-61]. It is noteworthy that PalA and Vps32, which are involved together with
410 PalB in pH-dependent proteolytic processing of PacC in other fungi, are dispensable in *M. oryzae* for

411 both alkaline pH adaptation and virulence(Fig.2), suggesting that they are not essential for generating
412 the different transcriptional regulator forms of PacC in *M. oryzae*. Whether the dispensability of
413 PalA and Vps32 is related with acidic processing of PacC in *M. oryzae* needs to be further addressed.

414 This study has revealed that full length PacC in *M. oryzae* also acts as a transcription repressor,
415 this is similar to the full-length form of Rim101p in *S. cerevisiae* [41]. In *C. albicans*, CaRim101p
416 also functions as both an activator and a repressor and has multiple forms although it is unclear
417 which form acts as a transcription repressor [43-44]. In *A. nidulans* there also is a full-length form of
418 pacC in the nucleus under alkaline pH [37], and it is reported that *A. nidulans* pacC can repress the
419 acid-expressed *gabA* gene by binding to its promoter regions and preventing binding of the
420 transcriptional activator *IntA* [62]. This suggests that in *A. nidulans* PacC can function as a
421 transcription repressor. However, it remains less clear how the two PacC isoforms recognize their
422 specific targets and achieve selectivity in transcriptional activation and repression.

423 Our results provide evidence that *M. oryzae* PacC activates genes that are specifically expressed
424 during biotrophic growth, and at the same time repress expression of genes that are related to
425 saprophytic growth (Fig.4A-4C). Over 2700 genes are differentially expressed in biotrophic IH of *M.*
426 *oryzae* when compared with a Δ pacC mutant (Fig. 4A; S1 Dataset). Therefore, more than 25% of the
427 total protein-encoding genes in *M. oryzae* genome are regulated by PacC. This is much higher than
428 the number regulated by PacC in other plant pathogenic fungi [54,56], where mycelium grown in
429 axenic conditions was used for RNA-Seq analysis. This is, however, the first time that biotrophic
430 infection has been analyzed for PacC regulation. We confirmed that *M. oryzae* PacC can bind to the
431 GCCAAG *cis*-element, as previously reported for *A. nidulans* PacC (Fig.5E, Fig.7B, S5B Fig., S6B
432 Fig., S7B Fig) [38]. By surveying PacC binding motifs in promoters of each differentially expressed
433 gene, we have identified nearly 1500 genes that are very likely to be directly regulated by PacC in *M.*
434 *oryzae* biotrophic IH (Fig 4A; S4 Dataset). It is notable that among the putatively direct targets of
435 PacC are genes enriched in those encoding extracellular and plasma membrane proteins (Fig 4D-4F;

436 S4 Dataset), that are likely to be involved in suppression of plant immunity, remodeling fungal cell
437 walls and acquisition of carbon and nitrogen sources from living host cells (Fig 4C-4D; S4 Dataset;
438 S5 Dataset) [50]. In particular, more than 80 previously characterized virulence genes appear to be
439 regulated by PacC (S6 Dataset), including effector protein genes and 12 genes that have been
440 identified to participate in acquisition and utilization of nutrients. Taken together, it seems likely that
441 an important role of PacC in *M. oryzae* is to regulate expression of genes that suppress plant
442 immunity, remodel the cell wall of invasive hyphae and facilitate acquisition and utilization of
443 nutrients to allow biotrophic growth in alkalinized host plant cells.

444 In conclusion, we propose a model for the regulation of hemibiotrophic growth of *M. oryzae* by
445 the PacC pH signaling pathway, as shown in Figure 8. Initially, *M. oryzae* penetration leads to pH
446 alkalinization in host cells around infection sites (Fig 8A). The alkalinized host environment is
447 sensed by Pal components of the PacC pathway, resulting in localization of PacC to the nucleus
448 where the activator isoform enhances gene expression associated with biotrophic growth, while the
449 repressor isoform represses genes associated with necrotrophic growth and conidiation (Fig 8B).
450 After extensive tissue colonization, *M. oryzae* induces disintegration and acidification of host plant
451 cells, which induces the two PacC isoforms to translocate from the nucleus thereby de-repressing
452 gene expression associated with necrotrophic growth and conidiation (Fig 8C). The shuttling of PacC
453 between the nucleus and cytoplasm according to pH in host tissue may thereby regulate the temporal
454 switch between biotrophic and necrotrophic growth that is essential for blast disease.

455 **Materials and Methods**

456 **Strains and culture conditions**

457 The P131 strain of *M. oryzae* was used for all genetic manipulation and infection assays [63]. S1528,
458 which has the opposite mating type to P131, was used only for genetic crossing and co-segregation
459 analyses, as previously described [64]. Strains 70-15 and DG-ZX-83, together with P131, were only
460 used to assay effect of pH on colony growth and conidiation. All the wild-type strains and
461 transformants (Supplemental Table 4) were maintained on oatmeal tomato agar (OTA) plates at
462 28°C, as described [63]. For assaying colony growth under normal condition, mycelial blocks ($\phi=5$
463 mm) were placed in the centre of complete medium (CM) plates, and cultured for 120 h at 28°C.
464 Conidia were produced on OTA, as previously reported [65]. For assaying the effect of pH on colony
465 growth and conidiation, CM plates and oatmeal agar plates were used, respectively, which were
466 adjusted to different pH with appropriate buffers, as described in Supplemental Figure 2.

467

468 **Plant infection and microscopy observations**

469 Rice and barley seedlings were grown, inoculated and incubated, as described for assaying virulence
470 [14,65]. Lesions on rice and barley leaves were examined at five days and three days post inoculation
471 (dpi), respectively. To assay virulence on wounded rice leaves, detached rice leaves were scratched
472 against leaf veins with a needle, then mycelial blocks ($\phi=2$ mm) were placed onto wounded sites,
473 and incubated in a moist chamber for 3 days.

474 Assays of the barley epidermal infection process, host-derived ROS generation and growth of
475 infection hyphae, were performed as described by Chen et al. [14]. To investigate subcellular
476 localization of PacC, microscopy was performed with a $\Delta pacC/GFP: pacC$ strain cultured in CM at
477 different pH, or inoculated onto barley epidermis. To visualize the viability of barley epidermal cells
478 at infection sites, Trypan blue staining of barley leaves was performed, as described previously [46].
479 All microscopic observations were made with a Nikon 90i epifluorescence microscope (Nikon,

480 Japan).

481

482 **Molecular manipulations with DNA and RNA**

483 Fungal genomic DNA was extracted, as described previously [66]. Total RNA was extracted with the
484 TRIzol Plus RNA Purification Kit (Life technologies, USA). Standard molecular procedures were
485 followed for plasmid preparation, Southern genomic DNA hybridization, and enzymatic digestion of
486 DNA [67]. TAIL-PCR was performed as described according to Liu et al. [48]. The qRT-PCR
487 reactions were performed with a ABI PRISM 7900HT system (Applied Biosystems, CA, USA) using
488 the SYBR® PrimeScript™ RT-PCR Kit (Takara, Dalian, China).

489

490 **Generation of gene deletion mutants and transformation**

491 Fungal protoplasts were isolated from *M. oryzae* mycelium that was cultured in liquid CM at 180 rpm
492 for 36 h and transformed as described [68]. CM plates supplemented with hygromycin B at 250
493 µg/ml (Roche, USA) or neomycin at 400 µg/ml (Amresco, USA), were used for selecting
494 hygromycin-resistant or neomycin-resistant transformants.

495 Mutants with targeted deletions of *PalI*, *PalA*, *PalB*, *PalC*, *PalF*, *PalH*, *PacC* and *Vps32* were
496 generated by one-step targeted gene replacement. To construct a gene replacement vector for each
497 gene, 1.5 kb upstream and 1.5 kb downstream sequences were amplified and cloned into pKNH [63].
498 The resulting vectors were independently transformed into P131. Transformants resistant to
499 hygromycin, but sensitive to neomycin, were subjected to screening by PCR. Gene deletion
500 candidates were further confirmed by Southern blot analysis.

501 For genetic complementation, genomic DNA fragments of individual *PalB*, *PalC*, *PalF*, *PalH*,
502 and *PacC* genes containing 1.5 kb promoter and 0.5 kb terminator regions were amplified and cloned
503 into pKN [63]. To generate the *eGFP-PacC* fusion construct pKGPacC⁵⁵⁹, a fragment amplified with
504 primers PacCNP5 and PacCNP3 was digested with *Xho*I and *Hind*III and cloned into pKNTG [63].
505 The same strategy was used to generate the pKGPacC²⁴⁵ and pKGPacC⁹⁶ constructs. pKGPacC⁵⁵⁹,
506 pKGPacC²⁴⁵ and pKGPacC⁹⁶ were independently transformed into a $\Delta pacC$ mutant to generate
507 strains NGP559 ($\Delta pacC/eGFP-PacC$), NGP245 and NGP96, respectively. pKGPacC⁵⁵⁹ was also

508 transformed into $\Delta palH$, $\Delta palF$, $\Delta palC$ and $\Delta palB$ to generate $\Delta palH/GFP:PalC$, $\Delta palF/GFP:PalC$,
509 $\Delta palC/GFP:PalC$ and $\Delta palB/GFP:PalC$ strains, respectively.
510

511 RNA-seq analysis

512 Total RNAs were isolated with the TRIzol Plus RNA Purification Kit (Life technologies, USA) from
513 epidermis of barley leaves that were inoculated with the P131 and the $\Delta pacC$ strain at 18 hpi. Each
514 RNA sample was subjected to DNase digestion (TaKaRa, Dalian, China), to remove DNA
515 contamination and then mRNA was purified with poly-T oligo-attached magnetic beads.
516 Construction of the libraries and RNA-Seq analysis were performed by Novogene Corporation
517 (Beijing, China) using an Illumina HiSeq 2000 platform (Illumina, Inc., USA). Raw reads were
518 filtered to remove adaptor and low-quality sequences. Clean reads were mapped to the P131 genome
519 [69] using Tophat2 [70], allowing up to two base mismatches. The Fragments Per Kilobase of
520 transcript sequence per Millions base pairs sequenced (FPKM) was used to indicate expression levels
521 of *M. oryzae* genes, which were calculated with Cuffdiff [71]. For either of the strains, two
522 independent sets of inoculated epidermis were prepared to generate the RNA-seq data. The
523 expression levels of *MGG_03982* (Actin gene) were used for normalizing different samples.
524 Differentially expressed genes between the wild type and the $\Delta pacC$ mutant were defined under the
525 criteria of the absolute log2 fold change value ≥ 0.5 , q value ≤ 0.05 and FPKM ≥ 2 in at least
526 one of the strains.
527

528 Intracellular pH measurement of barley leaf epidermal cells

529 The lower epidermis of barley leaves, inoculated with conidial suspension, was removed at
530 designated times to measure ambient pH in infected cells using
531 2',7'-bis-(2-carboxyethyl)-5-(and-6)-carboxyfluorescein-acetoxymethyl ester (BCECF-AM)
532 fluorescein as a pH indicator dye [45]. Emission intensities at 530 nm and 640 nm of the dye after

533 excitation at 488 nm were used to calculate pH, in accordance with a calibration curve between the
534 fluorescence ratio (F530/F640) and pH change, which was established with healthy barley leaf
535 epidermis, as described in the supplemental data. Three independent experiments were performed.
536 For each of the experiments, pH was measured in at least ten single plant cells underneath conidia or
537 appressoria or with invasive hyphae.

538

539 **Transcription activation assays**

540 To assay transcriptional activation activities of PacC, the full-length cDNA of *PacC* amplified with
541 primers PacC-F and PacC-R was digested with *Eco*RI and cloned into pGBKT7 (Clontech, USA) as
542 pBD-PacC⁵⁵⁹. A fragment encoding PacC²⁴⁵ and PacC⁹⁶ were amplified with primers
543 PacC-F/PacCR245 and PacC-F/PacCR96, and cloned into vector pGBKT7 as pBD-PacC²⁴⁵ and
544 pBD-PacC⁹⁶, respectively. These vectors were individually transformed into the yeast strain AH109.
545 Yeast cells were grown on SD-Trp and SD-Trp-His plates. Transformants with the empty vectors
546 pGBKT7 and pGBT9 were used as the negative and positive control, respectively. After 3 days
547 incubation at 28°C, X- α -gal was added to SD-Trp-His plates for assaying β -galactosidase activities.

548

549 **Electrophoretic mobility shift assays (EMSA)**

550 GST-fused PacC⁵⁵⁹, PacC²²² and PacC⁸⁰ proteins were individually expressed in the pGEX-4T-3
551 vector (Promega, USA) in *E. coli* BL21DE3 and purified, as described in supplementary data.
552 Double-stranded oligonucleotides were used as DNA templates for EMSA, which were formed by
553 mixing equal amounts of two single complementary oligonucleotides in the annealing buffer (0.2 M
554 Tris-HCl, 1 mM EDTA, 0.5 M NaCl, pH 8.0), heating for 5 min at 95°C, and cooling down to room
555 temperature. The double-stranded oligonucleotides were end-labeled with [α -³²P]-dCTP with the
556 Random Primer Labeling Kit (Takara, Dalian, China). The binding reaction (28 μ l) was performed in
557 binding buffer (10 mM Tris-HCl, pH 7.5, 5 mM NaCl, 1 mM DTT, 1 mM EDTA, 5% glycerol) with

558 50 ng of purified GST-fused PacC proteins and 2 pM labeled template DNA. 20 pM and 200 pM
559 un-labelled DNAs were used as 10 \times and 100 \times specific competitors, respectively. The samples were
560 separated on 8% native PAGE gels for 50 min, which were exposed to X-ray film for 1 h and
561 detected by a storage phosphor system (Cyclone, PerkinElmer, USA).

562

563 **Isolation of cytoplasmic and nuclear proteins from mycelia of *M. oryzae***

564 Cytoplasmic and nuclear proteins were isolated from protoplasts, as described with some
565 modifications [72]. The protoplasts were suspended in 400 μ l buffer A (10 mM HEPES-KOH, pH
566 7.9, 1.5 mM MgCl₂, 10 mM KCl, 0.5 mM DTT, 0.2 mM PMSF, 1 mg/ml leupeptin, 1 mg/ml
567 pepstatin) and vortexed six times. Each vortex lasted for 2 minutes, and 3 minute intervals were
568 allowed between each vortex to incubate the suspension on ice. After vortexing, the mixture was
569 centrifuged at 4,000 g for 15 min at 4°C to collect the supernatant as cytoplasmic proteins (CP). Then
570 200 μ l buffer B (20 mM HEPES-KOH, pH 7.9, 25% glycerol, 1.5 mM MgCl₂, 420 mM NaCl, 0.2
571 mM EDTA, 0.5 mM DTT, 0.2 mM PMSF, 1 mg/ml leupeptin, 1 mg/ml pepstatin) was added to
572 suspend the pellets on ice, which was vortexed again as mentioned above, and centrifuged at 12,000
573 g for 30 min at 4°C to collect the supernatant as nuclear proteins (NP). The CP and the NP were
574 mixed in ratio of 2:1 as the total proteins (TP). 30 μ l TP, 20 μ l CP, and 10 μ l NP were mixed with
575 equal volume 2 \times loading buffer and separated on 10% SDS-PAGE. Western blot was performed with
576 an anti-GFP antibody (Abmart, China).

577

578 **Plasmid Construction**

579 Cloning strategies for all plasmid constructions are described in the Extended Experimental
580 Procedures. All primers used and plasmids constructed were listed in Supplemental Tables 5 and 6,
581 respectively.

582

583 **Accession numbers**

584 Sequence data from this study can be found in the GenBank/EMBL data libraries under accession
585 number HQ889837 (*PacC*), HQ889838 (*PalH*), HQ889839 (*PalF*), HQ889840 (*PalC*), and
586 HQ889841 (*PalB*).

587

588 **Acknowledgments**

589 This work was supported by grants from the Ministry of Science and Technology
590 (2016YFD0300700, 2012CB114000), the Ministry of Agriculture and Rural Affairs (CARS-01-16,
591 201203014) and the Ministry of Education (B13006, IRT1042), China, to Y.-L.P. We thank
592 Professor Xinnian Dong at Duke University for her critical reading of the manuscript.

593 **Figure Legends**

594 **Fig 1. Barley epidermal cells are alkalinized during biotrophic growth but acidified during**
595 **necrotrophic growth of *M. oryzae*.** (A) Bright-field and Ratiometric confocal scanning laser
596 microscopy (CSLM) images of
597 2',7'-bis-(2-carboxyethyl)-5-(and-6)-carboxyfluorescein-acetoxymethyl ester (BCECF-AM) stained
598 barley epidermal cells infected with the wild-type *M. oryzae* strain P131 at indicated time points.
599 CO, conidium; AP, appressorium; PIH, primary IH; BIH, branched IH. Bar = 25 μ m. (B) Recorded
600 pH levels in barley epidermal cells invaded, (non-invaded) with the wild type and the $\Delta pacC$ mutant,
601 were calculated by analysing ratiometric CSLM images after BCECF-AM staining at 0-48 hpi. (C) A
602 Bright-field and Ratiometric CSLM image of BCECF-AM stained barley epidermal cells infected
603 with the $\Delta pacC$ mutant at 42 hpi. (D) Trypan Blue staining of infected plant cells was examined with
604 Nikon90i microscopy at different hpi. Bar = 25 μ m. (E) Bar charts showing the percentage of
605 infection sites in which the first, second and third infected cells were stained by Trypan Blue during
606 infection by the wild type strain and $\Delta pacC$ mutant. (F) Line graph showing inhibition of growth of
607 *M. oryzae* at pH < 5.5 or pH > 7.8. (G) Line graph showing inhibition of conidiation in *M. oryzae* at
608 pH > 7.8. Colony growth and conidiation were measured following growth on complete medium
609 (CM) and oat-broth medium, respectively, and were expressed in relation to the colony diameter or
610 conidiation at pH 6.5.

611

612 **Fig 2. PacC pathway deletion mutants are sensitive to alkaline pH and deficient in biotrophic**
613 **growth, conidiation and virulence.** (A) Colony growth of PacC pathway gene deletion mutants
614 under alkaline pH growth conditions, compared to the wild type (WT) P131. Strains were cultured
615 for 120 h on OTA medium and CM plates at pH 6.6 or 7.7. (B) Bar charts showing conidiation by
616 the same set of strains on OTA plates. Means and standard deviations were calculated from three
617 independent experiments. * $p < 0.01$, $n > 100$. (C) Blast disease lesions formed on barley leaves by

618 PacC pathway mutants at 5-day post-inoculation (dpi). (D) Micrographs showing development of
619 invasive hyphae (IH) formed by PacC pathway mutants in barley epidermal cells at 24 and 30 h post
620 inoculation (hpi). Bar = 20 μ m. (E) Bar chart showing the proportion of appressoria forming primary
621 IH or branched IH at 24 and 30 hpi. (F) Disease lesions formed by the wild type P131 and $\Delta pacC$
622 mutant on wounded rice leaves. (G) Micrographs showing that the arrested IH growth phenotype of
623 the $\Delta pacC$ mutant could not be restored by suppression of host reactive oxygen species (ROS) by
624 diphenyleneiodonium (DPI). A $\Delta alg3$ mutant was used as the control, which is deleted of the
625 α -1,3-mannosyltransferase gene, induces generation of ROS and is limited in biotrophic growth but
626 can be recovered by addition of DPI (ref. 9). Bar = 20 μ m.

627

628 **Fig 3. PacC Shows Distinct Subcellular Localization during Biotrophic and Necrotrophic**
629 **Growth.** (A) Bright-field and epifluorescence microscopy micrographs showing that PacC-GFP
630 localizes to the nucleus during biotrophic growth, but to the cytoplasm during necrotrophic growth
631 and asexual development. (B) Micrographs showing that alkaline pH > 7.2 induces nuclear
632 localization of PacC-GFP in the fungal mycelium. (C) Percentage of localization of PacC-GFP in
633 fungal mycelium cultured in different pH conditions. (D) Nuclear localization of PacC-GFP requires
634 the upstream *Pal* genes. PacC-GFP was introduced into $\Delta palH$, $\Delta palF$, $\Delta palC$, $\Delta palB$ mutants and
635 transformants grown at alkaline pH were visualized by epifluorescence microscopy. Photos were
636 recorded with a Nikon90i epifluorescence microscopy. Bar = 25 μ m.

637

638 **Fig 4. Global Transcriptional Profiling Reveals Major Families of PacC-Regulated Genes.** (A)
639 Bar charts showing the number of genes that are altered in expression in a $\Delta pacC$ mutant compared
640 to the wild type P131, in invasive hyphae (IH) at 18 hpi. Genes containing one or multiple
641 PacC-binding consensus GCCAAG in their promoters are indicated and regarded as PacC-directly
642 regulated genes. (B) Bar charts showing the highest expression stages of the PacC-directly activated

643 genes. (C) Bar charts showing the highest expression stages of the PacC-directly repressed genes.
644 (D) Bar charts showing the predicted subcellular localization of proteins encoded by PacC-directly
645 regulated genes in IH at18hpi. The bars marked ‘Whole genome’ indicates the proportion of genes in
646 the whole *M. oryzae* genome showing each predicted sub-cellular localization pattern. (E) Bar charts
647 showing the predicted functional annotations of putative extracellular proteins encoded by PacC
648 directly regulated genes in IH. (F) Bar charts showing functional annotations of predicted plasma
649 membrane proteins encoded by PacC directly-regulated genes in IH. Two independent duplicates of
650 RNA-seq data were obtained, and genes reproducibly altered in their expression with $\text{Log}_2 > 0.5$ or
651 < -0.5 , p value < 0.005 in the mutant were recorded as PacC- up or down regulated genes.

652

653 **Fig 5. PacC Exists as Both a Full-length Transcriptional Repressor and a Truncated**
654 **Transcriptional Activator.** (A) Western blot showing distinct PacC isoforms detected with
655 anti-GFP antibody in total (T), cytoplasmic (C) and nuclear (N) proteins extracted from mycelium of
656 NGP559 cultured at the pH indicated. Detection using an anti-GAPDH and an anti-histone H1
657 antibodies was used as the loading control for cytoplasmic and nuclear proteins, respectively. (B)
658 Schematic representation of GFP-PacC constructs transformed into the $\Delta pacC$ mutant. Dotted lines
659 indicate two putative cleavage sites. NP, native *PacC* promoter; ZF, zinc finger domains. (C)
660 Western blot showing PacC isoforms detected with an anti-GFP antibody in nuclear proteins of
661 transformants NGP96, NGP245 and NGP559 cultured at pH 7.7. (D) Yeast transcription activation
662 assay showing pBD-PacC⁵⁵⁹, pBD-PacC²⁴⁵ and pBD-PacC⁹⁶ grown on SD-Trp-His plates and
663 β -galactosidase activity on SD-Trp-His plus X-gal plates. pGBT9 and pGBT7 were the positive
664 and negative controls, respectively. (E) Electrophoretic mobility shift assay of GST-PacC559,
665 GST-PacC222 and GST-PacC80 showing potential binding to a ³²P-labelled 4 \times GCCAAG consensus
666 sequence. (F), (G) and (H) show colony growth by the wild type P131, the $\Delta pacC$ mutant, and
667 transformants NGP96, NGP245 and NGP559 on OTA and CM at the indicated pH, conidiation of

668 the same strains on OTA and blast disease assays.

669

670 **Fig 6. Bar charts showing qRT-PCR analysis to show genes down-regulated by PacC⁵⁵⁹ or**
671 **up-regulated by PacC²²².** (A) Bar charts showing qRT-PCR analysis of genes up-regulated in the
672 $\Delta pacC$ mutant and NGP245, but down-regulated in the wild type and NGP559. (B) Genes
673 down-regulated in the $\Delta pacC$ mutant, but up-regulated in the wild type, NGP245 and NGP559. The
674 relative expression levels of each gene were assayed by qRT-PCR with total RNA isolated from
675 mycelium cultured under pH 7.7. For each gene, its expression level in the wild type P131 cultured
676 in pH 7.7 was arbitrarily set as 1. WT, the wild-type P131; $\Delta pacC$, *PacC* deletion mutant; NGP245,
677 a transformant of the $\Delta pacC$ mutant with *eGFP-PacC²⁴⁵* construct; NGP559, a transformant of the
678 $\Delta pacC$ mutant with *eGFP-PacC⁵⁵⁹* construct.

679

680 **Fig 7. *PAG1* is positively regulated by PacC and important for biotrophic growth of *M. oryzae*.**
681 (A) Expression of *PAG1* in mycelium of WT P131, $\Delta pacC$, NGP239, and NGP559. For the Q-PCR,
682 the expression level of P131 cultured at pH 5.5 was arbitrarily set to 1. (B) PacC binds to GCCAAG
683 motifs in the *PAG1* promoter. Purified GST-PacC²²² protein was used to detect binding of putative
684 PacC binding motifs. Probes 1 and 2 contain predicted PacC-binding motifs and were prepared by
685 labelling with ³²P-dCTP and incubated with GST-PacC²²² for 30 min, before loading a native-PAGE
686 gel. For competition experiments, 100x or 10x concentrations of un-labelled Probe 1 were mixed
687 with the GST-PacC²²² protein for 30 min before incubation with ³²P-dCTP-labelled probes. (C) WT
688 and $\Delta pag1$ are same in colony growth on OTA plates. (D) WT and $\Delta pag1$ are equivalent in
689 conidiation. (E) Reduced virulence of $\Delta pag1$ mutant compared to WT. (F) Infection assays of WT
690 and $\Delta pag1$ on barley epidermis. (G) Arrested biotrophic growth of $\Delta pag1$ compared to WT. Bar = 25
691 μm .

692

693 **Fig 8. A Model for PacC-Dependent Regulation of Gene Expression Associated with the**
694 **Biotrophic/Necrotrophic Switch during Infection of *M. oryzae*.** (A) Infected plant cells are
695 alkalinized during the early biotrophic growth of *M. oryzae* and then become acidified during the
696 later necrotrophic growth. (B) During biotrophic growth, the PacC⁵⁵⁹ and PacC²²² transcription factor
697 isoforms localize to the nucleus, where PacC⁵⁵⁹ acts as a transcriptional repressor to repress
698 expression of genes associated with conidiation and necrotrophic growth, including *PRG1*, *HTF1*,
699 and *PIG1* while PacC²²² acts as a transcriptional activator to activate genes associated with
700 biotrophic growth. (C) As host cells become acidified and lose viability, the PacC functional
701 isoforms exit from the nucleus thereby de-repressing expression of genes related to necrotrophic
702 growth and conidiation.

703 **References**

704

705 1. Oliver, R.P., and Ipcho, S.V. (2004). *Arabidopsis* pathology breathes new life into the
706 necrotrophs-vs.-biotrophs classification of fungal pathogens. *Mol. Plant. Pathol.* 5, 347–352.

707 2. Rowe, H.C., and Kliebenstein, D.J. (2010). All mold is not alike: the importance of intraspecific
708 diversity in necrotrophic plant pathogens. *PLoS Pathog.* 6, e1000759.

709 3. Spanu, P.D. (2012). The genomics of obligate (and nonobligate) biotrophs. *Ann. Rev.*
710 *Phytopathol.* 50, 91–109.

711 4. Fernandez, J., Marroquin-Guzman, M. and Wilson R.A. (2014) Mechanisms of nutrient
712 acquisition and utrilization during fungal infections of leaves. *Annu. Rev. Phytopathol.*
713 52:155-74

714 5. Glazebrook, J. (2005). Contrasting mechanisms of defense against biotrophic and necrotrophic
715 pathogens. *Annu. Rev. Phytopathol.* 43, 205–227.

716 6. Sun, G., Elowsky, C., Li, G. and Wilson, R.A. (2018) TOR-autophagy branch signaling via Imp1
717 dictates plant-microbe biotrophic interface longevity. *PLoS Genetics* 14: e1007814

718 7. Dean, R., Van Kan, J.A., Pretorius, Z.A., Hammond-Kosack, K.E., Di Pietro, A., Spanu, P.D.,
719 Rudd, J.J., Dickman, M., Kahmann, R., Ellis, J., and Foster, G.D. (2012). The Top 10 fungal
720 pathogens in molecular plant pathology. *Mol. Plant Pathol.* 13(4), 414–430.

721 8. Fernandez, J. and Orth, K. (2018) Rice of a Cereal Killer: The biology of *Magnaporthe oryzae*
722 biotrophic growth. *Trends Microbiol.* 26, 582-97.

723 9. Kankanala, P., Czymmek, K., and Valent, B. (2007). Roles for rice membrane dynamics and
724 plasmodesmata during biotrophic invasion by the blast fungus. *Plant Cell* 19, 706–724.

725 10. Wilson, R. A., and Talbot, N. J. (2009). Under pressure: investigating the biology of plant
726 infection by *Magnaporthe oryzae*. *Nat. Rev. Microbiol.* 7, 185–195.

727 11. Giraldo, M.C., Dagdas, Y.F., Gupta, Y.K., Mentlak, T.A., Yi, M., Martinez-Rocha, A.L., Saitoh,

728 H., Terauchi, R., Talbot, N.J., and Valent, B. (2013). Two distinct secretion systems facilitate
729 tissue invasion by the rice blast fungus *Magnaporthe oryzae*. *Nat. Commun.* 4, 1996.

730 12. Khang, C.H., Berruyer, R., Giraldo, M.C., Kankanala, P., Park, S.Y., Czymbek, K., Kang, S.,
731 and Valent, B. (2010). Translocation of *Magnaporthe oryzae* effectors into rice cells and their
732 subsequent cell-to-cell movement. *Plant Cell* 22, 1388-1403.

733 13. Mentlak, T.A., Kombrink, A., Shinya, T., Ryder, L.S., Otomo, I., Saitoh, H., Terauchi, R.,
734 Nishizawa, Y., Shibuya, N., Thomma, B.P., and Talbot, N.J. (2012). Effector-mediated
735 suppression of chitin-triggered immunity by *Magnaporthe oryzae* is necessary for rice blast
736 disease. *Plant Cell* 24, 322–335.

737 14. Chen, X.L., Shi, T., Yang, J., Shi, W., Gao, X.S., Chen, D., Xu, X.W., Xu, J.R., Talbot, N.J., and
738 Peng, Y.L. (2014). N-glycosylation of effector proteins by an α -1,3-mannosyltransferase is
739 required for the rice blast fungus to evade host innate immunity. *Plant Cell* 26(3), 1360-1376.

740 15. Sakulkoo, W., Oses-Ruiz, M., Oliveira Garcia, E., Soanes, D.M., Littlejohn, G.R., Hacker, C.,
741 Correia, A., Valent, B., and Talbot, N.J. (2018). A single fungal MAP kinase controls plant
742 cell-to-cell invasion by the rice blast fungus. *Science* 359, 1399–1403.

743 16. Marroquin-Guzman, M., Hartline, D., Wright, J.D., Elowsky, C., Bourret, T.J., and Wilson, R.A.
744 (2017). The *Magnaporthe oryzae* nitrooxidative stress response suppresses rice innate immunity
745 during blast disease. *Nat. Microbiol.* 2, 17054.

746 17. Vylkova, S. (2017). Environmental pH modulation by pathogenic fungi as a strategy to conquer
747 the host. *PLoS Pathog.* 13, e1006149.

748 18. Felix, G., Regenass, M., and Boller, T. (1993). Specific perception of subnanomolar
749 concentrations of chitin fragments by tomato cells: induction of extracellular alkalinization,
750 changes in protein phosphorylation, and establishment of a refractory state. *Plant J.* 4, 307–316.

751 19. Felle, H.H. (2001). pH: signal and messenger in plant cells. *Plant Biol.* 3, 577–591.

752 20. Zipfel, C., Kunze, G., Chinchilla, D., Caniard, A., Jones, J.D., Boller, T., and Felix G. (2006).

753 Perception of the bacterial PAMP EF-Tu by the receptor EFR restricts *Agrobacterium*-mediated
754 transformation. *Cell* 125, 749–760.

755 21. Gust, A. A., Biswas, R., Lenz, H.D., Rauhut, T., Ranf, S., Kemmerling, B., Götz, F., Glawischnig,
756 E., Lee, J., Felix, G., and Nürnberg, T. (2007). Bacteria-derived peptidoglycans constitute
757 pathogen-associated molecular patterns triggering innate immunity in *Arabidopsis*. *J. Biol. Chem.*
758 282, 32338–32348.

759 22. Fernandes, T.R., Segorbe, D., Prusky, D., and Di Pietro, A. (2017). How alkalinization drives
760 fungal pathogenicity. *PLoS Pathog.* 13, e1006621.

761 23. Bateman, D.F., and Beer, S.V. (1965). Simultaneous production and synergistic action of oxalic
762 acid and polygalacturonase during pathogenesis by *Sclerotium rolfsii*. *Phytopathology* 55, 204–
763 211.

764 24. Cessna, S., Sears, V., Dickman, M., and Low, P. (2000). Oxalic acid, a pathogenicity factor of
765 *Sclerotinia sclerotiorum*, suppresses the host oxidative burst. *Plant Cell* 12, 2191–2199.

766 25. Masachis, S., Segorbe, D., Turrà, D., Leon-Ruiz, M., Fürst, U., Ghalid, M.E., Leonard, G.,
767 López-Berges, M.S., Richards, T.A., Felix, G., and Pietro, A.D. (2016). A fungal pathogen
768 secretes plant alkalinizing peptides to increase infection. *Nature Microbiol.* 1, 16043.

769 26. Peñalva, M.A., Tilburn, J., Bignell, E., and Arst, H.N., Jr. (2008). Ambient pH gene regulation in
770 fungi: making connections. *Trends Microbiol.* 16, 291–300.

771 27. Galindo, A., Calcagno-Pizarelli, A.M., Arst, H.N. Jr., and Peñalva, M.A. (2012) An ordered
772 pathway for the assembly of ESCRT-containing fungal ambient pH signalling complexes at the
773 plasma membrane. *J Cell Sci.* 125, 1784–1795.

774 28. Calcagno-Pizarelli, A.M., Negrete-Urtasun, S., Denison, S.H., Rudnicka, J.D., Bussink, H.J.,
775 Munera-Huertas, T., Stanton, L., Hervas-Aguilar, A., Espeso, E.A., Tilburn, J., Arst, H.N. Jr.,
776 and Peñalva M.A. (2007). Establishment of the ambient pH signaling complex in *Aspergillus*
777 *nidulans*: PalI assists plasma membrane localization of PalH. *Eukaryot Cell* 6, 2365–2375.

778 29. Herranz, S., Rodriguez, J.M., Bussink, H.J., Sanchez-Ferrero, J.C., Arst, H.N., Jr., Peñalva, M.A.,
779 and Vincent, O. (2005). Arrestin-related proteins mediate pH signaling in fungi. Proc Natl Acad
780 Sci U S A. 102, 12141–12146.

781 30. Hervas-Aguilar, A., Galindo, A., and Peñalva, M.A. (2010). Receptor-independent Ambient pH
782 signaling by ubiquitin attachment to fungal arrestin-like PalF. J Biol Chem. 285(23),
783 18095-18102.

784 31. Galindo, A., Hervas-Aguilar, A., Rodriguez-Galan, O., Vincent, O., Arst, H.N., Jr., Tilburn, J.,
785 and Peñalva, M.A. (2007). PalC, one of two Bro1 domain proteins in the fungal pH signalling
786 pathway, localizes to cortical structures and binds Vps32. Traffic 8, 1346-1364.

787 32. Denison, S.H., Orejas, M., and Arst, H.N., Jr. (1995). Signaling of ambient pH in *Aspergillus*
788 involves a cysteine protease. J Biol Chem. 270, 28519–28522.

789 33. Peñas, M.M., Hervás-Aguilar, A., Munéra-Huertas, T., Reoyo, E., Peñalva, M.A., Arst, H.N., Jr.,
790 and Tilburn, J. (2007). Further characterization of the signaling proteolysis step in the *Aspergillus*
791 *nidulans* pH signal transduction pathway. Eukaryot. Cell 6, 960–970.

792 34. Espeso, E.A., Roncal, T., Diez, E., Rainbow, L., Bignell, E., Alvaro, J., Suarez, T., Denison, S.H.,
793 Tilburn, J., Arst, H.N. Jr., and Peñalva, M.A. (2000). On how a transcription factor can avoid its
794 proteolytic activation in the absence of signal transduction. EMBO J. 19, 719-728.

795 35. Diez, E., Alvaro, J., Espeso, E.A., Rainbow, L., Suarez, T., Tilburn, J., Arst, H.N., Jr., and
796 Peñalva, M.A. (2002). Activation of the *Aspergillus* PacC zinc finger transcription factor requires
797 two proteolytic steps. EMBO J. 21, 1350–1359.

798 36. Vincent, O., Rainbow, L., Tilburn, J., Arst, H.N., and Peñalva, M.A. (2003). YPXL/I is a protein
799 interaction motif recognized by *Aspergillus* PalA and its human homologue, AIP1/Alix. Mol Cell
800 Biol. 23, 1647–1655.

801 37. Mingot, J.M., Espeso, E.A., Diez, E., and Peñalva, M.A. (2001). Ambient pH signaling regulates
802 nuclear localization of the *Aspergillus nidulans* PacC transcription factor. Mol Cell Biol. 21,

803 1688–1699.

804 38. Espeso, E.A., Tilburn, J., Sanchez-Pulido, L., Brown, C.V., Valencia, A., Arst, H.N.Jr, and
805 Peñalva, M.A. (1997). Specific DNA recognition by the *Aspergillus nidulans* three zinc finger
806 transcription factor PacC. *J. Mol. Biol.* 274, 466–480.

807 39. Fernandez-Martinez, J., Brown, C.V., Diez, E., Tilburn, J., Arst, H.N., Jr., Peñalva, M.A., and
808 Espeso, E.A. (2003). Overlap of nuclear localisation signal and specific DNA-binding residues
809 within the zinc finger domain of PacC. *J Mol Biol.* 334, 667–684.

810 40. Davis, D. (2003). Adaptation to environmental pH in *Candida albicans* and its relation to
811 pathogenesis. *Curr Genet.* 44, 1–7.

812 41. Lamb, T. M., and Mitchell, A. P. (2003). The transcription factor Rim101p governs ion tolerance
813 and cell differentiation by direct repression of the regulatory genes *NRG1* and *SMPI* in
814 *Saccharomyces cerevisiae*. *Mol. Cell Biol.* 23, 677–686.

815 42. Li, M., Martin, S.J., Bruno, V.M., Mitchell, A.P., and Davis, D.A. (2004). *Candida albicans*
816 Rim13p, a protease required for Rim101p processing at acidic and alkaline pHs. *Eukaryot Cell.* 3,
817 741–751.

818 43. Baek, Y.U., Martin, S.J., and Davis, D.A. (2006). Evidence for novel pH-dependent regulation of
819 *Candida albicans* Rim101, a direct transcriptional repressor of the cell wall beta-glycosidase
820 Phr2. *Eukaryot. Cell* 5, 1550–1559.

821 44. Ramon, A.M., and Fonzi, W.A. (2003). Diverged binding specificity of Rim101p, the *Candida*
822 *albicans* ortholog of PacC. *Eukaryot Cell.* 2, 718–728.

823 45. Ozkan, P., and Mutharasan, R. (2002). A rapid method for measuring intracellular pH using
824 BCECF-AM. *Biochim. Biophys Acta* 1572, 143–148.

825 46. Lipka, V., Dittgen, J., Bednarek, P., Bhat, R., Wiermer, M., Stein, M., Landtag, J., Brandt, W.,
826 Rosahl, S., Scheel, D., Llorente, F., Molina, A., Parker, J., Somerville, S., and Schulze-Lefert, P.
827 (2005). Pre- and postinvasion defenses both contribute to nonhost resistance in

828 828 *Arabidopsis*. Science 310, 1180-1183.

829 829 47. Chen, X.L., Yang, J., and Peng, Y.L. (2011). Large-scale insertional mutagenesis in
830 830 *Magnaporthe oryzae* by *Agrobacterium tumefaciens*-mediated transformation. Methods Mol.
831 831 Biol. 722, 213–224.

832 832 48. Liu, Y. G., Mitsukawa, N., Oosumi, T., and Whittier, R.F. (1995). Efficient isolation and
833 833 mapping of *Arabidopsis thaliana* T-DNA insert junctions by thermal asymmetric interlaced PCR.
834 834 Plant J. 8, 457–463.

835 835 49. Peñalva, M.A., Lucena-Agell, D., and Arst, H.N.Jr. (2014). Liaison alcaline: Pals entice
836 836 non-endosomal ESCRTs to the plasma membrane for pH signaling. Curr. Opin. Microbiol. 22,
837 837 49–59.

838 838 50. Strasser, K., McDonnell, E., Nyaga, C., Wu, M., Wu, S., Almeida, H., Meurs, M.J., Kosseim, L.,
839 839 Powlowski, J., Butler, G. and Tsang, A. (2015). mycoCLAP, the database for characterized
840 840 lignocellulose-active proteins of fungal origin: resource and text mining curation support.
841 841 Database (Oxford) 8, 2015.

842 842 51. Liu W, Xie S, Zhao X, Chen X, Zheng W, Lu G. Wang Z. (2010) A homeobox gene is essential
843 843 for conidiogenesis of the rice blast fungus *Magnaporthe oryzae*. Mol Plant Microbe Interact
844 844 23(4): 366-375.

845 845 52. Tsuji G, Kenmochi Y, Takano Y, Sweigard J, Farrall L, et al. (2000) Novel fungal transcriptional
846 846 activators, Cmr1p of *Colletotrichum lagenarium* and pig1p of *Magnaporthe grisea*, contain
847 847 Cys₂His₂ zinc finger and Zn(II)₂Cys₆ binuclear cluster DNA-binding motifs and regulate
848 848 transcription of melanin biosynthesis genes in a developmentally specific manner. Mol Microbiol
849 849 38, 940-954.

850 850 53. Landraud, P., Chuzeville, S., Billon-Grande, G., Poussereau, N., and Bruel, C. (2013).
851 851 Adaptation to pH and role of PacC in the rice blast fungus *Magnaporthe oryzae*. PLoS ONE 8,
852 852 e69236.

853 54. Alkan, N., Meng, X., Friedlander, G., Reuveni, E., Sukno, S., Sherman, A., Thon, M., Fluhr, R.,
854 and Prusky, D. (2013). Global aspects of pacC regulation of pathogenicity genes in
855 *Colletotrichum gloeosporioides* as revealed by transcriptome analysis. Mol. Plant Microbe
856 Interact. 26(11), 1345-1358.

857 55. Caracuel, Z., Roncero, M.I., Espeso, E.A., Gonzalez-Verdejo, C.I., Garcia-Maceira, F.I., and Di
858 Pietro, A. (2003). The pH signalling transcription factor PacC controls virulence in the plant
859 pathogen *Fusarium oxysporum*. Mol Microbiol 48, 765-779.

860 56. Chen, Y., Li, B.Q., Xu, X.D., Zhang, Z.Q., and Tian, S.P. (2018). The pH-responsive PacC
861 transcription factor plays pivotal roles in virulence and patulin biosynthesis in *Penicillium*
862 *expansum*. Environ. Microbiol. 20, 4063–4078.

863 57. Rollins, J.A., and Dickman, M.B. (2001). PH signaling in *Sclerotinia sclerotiorum*: Identification
864 of a pacC/RIM1 Homolog. Appl Environ Microb 67, 75-81.

865 58. You, B.J., Choquer, M., and Chung, K.R. (2007). The *Colletotrichum acutatum* gene encoding a
866 putative pH-responsive transcription regulator is a key virulence determinant during fungal
867 pathogenesis on citrus. Mol Plant Microbe Interact. 20, 1149-1160.

868 59. Lucena-Agell, D, Hervas-Aguilar, A., Munera-Huertas, T., Pougovkina, O., Rudnicka, J.,
869 Galindo, A., Tilburn, J., Arst, H.N. Jr., and Peñalva, M.A. (2016). Mutational analysis of the
870 *Aspergillus* ambient pH receptor PalH underscores its potential as a target for antifungal
871 compounds, Mol Microbiol, 101, 982-1002.

872 60. Li W. and Mitchell A. P. (1997). Proteolytic Activation of Rimlp, a Positive Regulator of Yeast
873 Sporulation and Invasive Growth. Genetics 145, 63-73

874 61. Futai E., Maeda T., Sorimachi H., Kitamoto K., Ishiura S., Suzuki K. (1999). The protease
875 activity of a calpain-like cysteine protease in *Saccharomyces cerevisiae* is required for alkaline
876 adaptation and sporulation. Mol Gen Genet 260, 559–568.

877 62. Espeso, E.A., and Arst, H.N. Jr., (2000). On the mechanism by which alkaline pH prevents
878 expression of an acid-expressed gene. Mol Cell Biol. 20, 3355–3363.

879 63. Yang, J., Zhao, X.Y., Sun, J., Kang, Z.S., Ding, S.L., Xu, J.R., and Peng, Y.L. (2010) A novel
880 protein Com1 is required for normal conidium morphology and full virulence in *Magnaporthe*
881 *oryzae*. *Mol. Plant Microbe Interact.* 23, 112-123.

882 64. Talbot, N.J., Kershaw, M.J., Wakley, G.E., De Vries, O.M.H., Wessels, J.G.H., and Hamer, J.E.
883 (1996). *MPG1* encodes a fungal hydrophobin involved in surface interactions during
884 infection-related development of *Magnaporthe grisea*. *Plant Cell* 8, 985-999.

885 65. Peng, Y.L., and Shishiyama, J. (1988). Temporal sequence of cytological events in rice leaves
886 infected with *Pyricularia oryzae*. *Can. J. Bot.* 66, 730–735.

887 66. Xu, J.R., and Hamer, J.E. (1996). MAP kinase and cAMP signaling regulate infection structure
888 formation and pathogenic growth in the rice blast fungus *Magnaporthe grisea*. *Genes Dev.*
889 10(21), 2696-2706.

890 67. Sambrook, J., and Russell, D.W. (2001). Molecular cloning: A laboratory manual. (Cold Spring
891 Harbor, NY: Cold Spring Harbor Laboratory Press).

892 68. Park, G., Xue, C., Zhao, X., Kim, Y., Orbach, M., Xu, J.R. (2006) Multiple upstream signals
893 converge on the adaptor protein Mst50 in *Magnaporthe grisea*. *Plant Cell*. 18, 2822-2835.

894 69. Xue, M., Yang, J., Li, Z., Hu, S., Yao, N., Dean, R.A., Zhao, W., Shen, M., Zhang, H., Li, C.,
895 Liu, L., Cao, L., Xu, X., Xing, Y., Hsiang, T., Zhang, Z., Xu, J.R., and Peng, Y.L. (2012).
896 Comparative analysis of the genomes of two field isolates of the rice blast fungus *Magnaporthe*
897 *oryzae*. *PLoS Genet.* 8, e1002869.

898 70. Kim, D., Pertea, G., Trapnell, C., Pimentel, H., Kelley, R., and Salzberg. S.L. (2013). TopHat2:
899 accurate alignment of transcriptomes in the presence of insertions, deletions and gene fusions.
900 *Genome Biol.* 14(4), R36.

901 71. Trapnell, C., Williams, B.A., Pertea, G., Mortazavi, A., Kwan, G., van Baren, M.J., Salzberg,
902 S.L., Wold, B.J., and Pachter, L. (2010). Transcript assembly and quantification by RNA-Seq
903 reveals unannotated transcripts and isoform switching during cell differentiation. *Nat. Biotechnol.*

904 28, 511-515.

905 72. Vanheeswijck, R. and Hynes, M.J. (1991). The amdR product and a CCAAT-binding factor bind

906 to adjacent, possibly overlapping DNA sequences in the promoter region of the *Aspergillus*

907 *nidulans* amdS gene. Nucleic Acids Res. 19, 2655-2660.

908 **Supporting Information**

909 **S1 Fig. *In situ* pH calibration curve and three-dimension visualization of cellular pH in barley**
910 **leaf epidermal cells infected with *M. oryzae*.**

911 (A) A calibration curve of the fluorescence ratio (F_{530}/F_{640}) against pH changes was established by
912 using epidermis of un-inoculated barley leaves. The epidermis was pre-treated for 15 min with
913 Nigericin (Invitrogen, USA) dissolved in buffers (pH 6.0, 6.5, 7.0, 7.5 and 8.0) and then added with
914 the dye, BCECF-AM fluorescein, before visualization by laser scanning confocal microscopy.
915 Emission intensities at 530 nm and 640 nm of the dye after excitation at 488 nm, were recorded with
916 a Nikon A1 Laser scanning confocal microscope (Nikon, Japan). Error bars represent the standard
917 deviation of 14 images taken from 7 different epidermal cells. (B) Three-dimension visualization of
918 cellular pH in barley leaf epidermal cells infected by *M. oryzae*. A bright-field and Ratiometric
919 CSLM image of BCECF-AM stained barley epidermal cells infected by the wild type P131 at 18 hpi
920 (up panel) and at 36 hpi (bottom panel). Cross sections were also made, as indicated in the red and
921 blue lines and are shown at the right and bottom, respectively. PIH, primary infection hyphae; BIH,
922 branched infection hyphae; CSLM: confocal scanning laser microscopy; Bar = 25 μ m. BCECF-AM:
923 2',7'-bis-(2-carboxyethyl)-5-(and-6)-carboxyfluorescein-acetoxymethyl ester.

924

925 **S2 Fig. Effect of pH on colony growth and conidiation of *M. oryzae* isolates 70-15 and**
926 **DG-ZX-83.** Colony growth and conidiation by *M. oryzae* were assayed on complete medium (CM)
927 and oat broth (OBA) medium, respectively. OBA medium was made from agar (16g/L) and oat
928 broth, which was prepared by boiling flattened oats (10 g/L) in water for 20min and filtering with
929 gauze. CM and OBA were adjusted to pH 5.5 with 0.2M sodium acetate buffer (final concentration
930 25mM), to pH 6.0 - 7.5 with 0.2M phosphate buffer solution (final PO_4^{3-} -concentration 50mM), or to
931 pH 7.8 to 8.5 with 0.2M Tris-HCl buffer (final concentration to 50mM). (A) Graphs showing colony
932 growth of 70-15 and DG-ZX-83 under different pH conditions. (B) Conidiation of 70-15 and

933 DG-ZX-83 under different pH conditions. (C) Colony morphology of 70-15 and DG-ZX-83 under
934 different pH conditions. (D) Micrographs of conidium formation of 70-15 and DG-ZX-83 under
935 different pH conditions. Colony diameter and conidium number formed under individual pH
936 conditions were normalized against those formed at pH 6.5. Bar = 20 μ m.

937

938 **S3 Fig. Phenotypes of nine *Agrobacterium tumefaciens*-mediated transformation (ATMT)**
939 **mutants of *M. oryzae* and positions of their T-DNA insertion sites.** (A) Colony growth of ATMT
940 mutants compared with the wild type P131 on oatmeal tomato agar (OTA) plate and CM plates
941 buffered at pH 6.6 and 7.7. Colonies were photographed at 120 hpi. (B) Conidia production of
942 ATMT mutants as compared with the wild type P131. Conidia were harvested from the strains that
943 were cultured on OTA plates ($\Phi=6$ cm). Means and standard deviation were calculated from three
944 independent experiments. ** $p < 0.01$, $n > 100$. (C) Virulence of ATMT mutants compared to the
945 wild type P131. Conidia of P131 and the mutants with concentration of 5×10^4 spores/ml in 0.025%
946 Tween 20 were used to spray the barley leaves. Infected leaves were photographed at 5 dpi. (D)
947 Diagram showing T-DNA integration sites in the nine alkaline pH-sensitive ATMT mutants. The
948 insertion sites are marked with black arrows and numbers indicating the relative distance to the ATG
949 codon of corresponding genes.

950

951 **S4 Fig. Strategies for generating gene deletion mutants of the PacC pathway and**
952 **corresponding Southern blot analysis.** To generate gene replacement constructs, approximately 1.5
953 kb of upstream and 1.5 kb of downstream flanking sequences (shaded in gray) of each targeted gene
954 were amplified with specific primer pairs listed in Table S9. The resulting PCR products were cloned
955 into restriction enzyme sites flanking the hygromycin phosphotransferase (*hph*) gene of plasmid
956 pKNH to generate specific gene replacement vectors (left panes of A-G). The right panels in (A)-(G)
957 are images of Southern blots of the resulting knockout mutants hybridized with the probes marked in

958 the schematic drawings. Genomic DNAs were isolated from the wild-type strain P131 (WT) and two
959 or three representative knockout mutants for each gene. B, *Bam*HI; C, *Clal*; E, *Eco*RI; H, *Hind*III; K,
960 *Kpn*I; P, *Pst*I; S, *Spe*I; SA, *Sac*I; X, *Xho*I.

961

962 **S5 Fig. *PRG1* is negatively regulated by PacC and its overexpression results in smaller colony
963 growth.** (A) Expression of *PRG1* in mycelia of WT P131, $\Delta pacC$, NGP239, and NGP559. (B) PacC
964 binding to the GCCAAG consensus from the promoter of *PRG1*. (C) Colonies of P131 (WT), the
965 $\Delta prg1$ mutant, RP8 and MC1. RP8 and MC1 are a *PRG1* overexpression transformant driven by the
966 RP27 promoter and a transformant expressing the mutant allele of *PRG1* with the PacC-binding site
967 changed from GCCAAG to CTGCAG in its native promoter of the $\Delta prg1$ mutant, respectively. (D)
968 Colony diameter of following strains: WT, the $\Delta prg1$ mutant, transformants RP2, RP8, RP12, RP14,
969 RP15, RP18, RP20 that overexpress *PRG1* driven by the RP27 promoter, transformants MC1, MC6,
970 MC11, MC19, MC20, MC21, MC28 that over-express *PRG1* driven by its native promoter with the
971 PacC-binding cis-element mutated as described in (C). (E) Expression levels of *PRG1* in the same set
972 of strains described above. (F) Conidiation of WT and the $\Delta prg1$ mutant. (G) Virulence of WT and
973 the $\Delta prg1$ mutant on barley leaves.

974

975 **S6 Fig. *HTF1* is negatively regulated by PacC559.** (A) Quantitative RT-PCR analysis of *HTF1*
976 expressed in mycelia of different strains under alkaline and acidic pH. (B) PacC binding to the
977 GCCAAG consensus from the promoter of *HTF1*.

978

979 **S7 Fig. *PIG1* is negatively regulated by PacC.** (A) Quantitative RT-PCR analysis of *PIG1*
980 expressed in mycelia of different strains under alkaline and acidic pH. (B) PacC binding to the
981 GCCAAG consensus from the promoter of *PIG1*.

982

983 **S1 Table.** Co-segregation of the phenotype changes with the hygromycin resistance in the nine
984 alkaline pH-sensitive mutants.

985 **S2 Table.** Colony sizes of the WT strain and deletion mutants grown at different ambient pH.

986 **S3 Table.** Putative PacC cleavage sites predicted by the Peptidecutter.

987 **S4 Table.** *M. oryzae* Strains used in this study.

988 **S5 Table.** Plasmids used in this study.

989 **S6 Table.** Primers used in this study.

990 **S1 Dataset.** Genes expressed in biotrophic infection hyphae of the wild type and $\Delta pacC$ strains at
991 18hpi.

992 **S2 Dataset.** Expression levels in other stages of the PacC-activated genes during biotrophic growth.

993 **S3 Dataset.** Expression levels in other stages of the PacC directly suppressed genes during
994 biotrophic growth.

995 **S4 Dataset.** Annotations of genes directly regulated by PacC in the biotrophic infection hyphae.

996 **S5 Dataset.** Glycoside hydrolases may act on plant cell wall polysaccharides to provide carbon
997 sources for biological growth of infection hyphae

998 **S6 Dataset.** Previously reported pathogenicity-important genes that are differentially regulated by
999 PacC in the biotrophic infection hyphae.

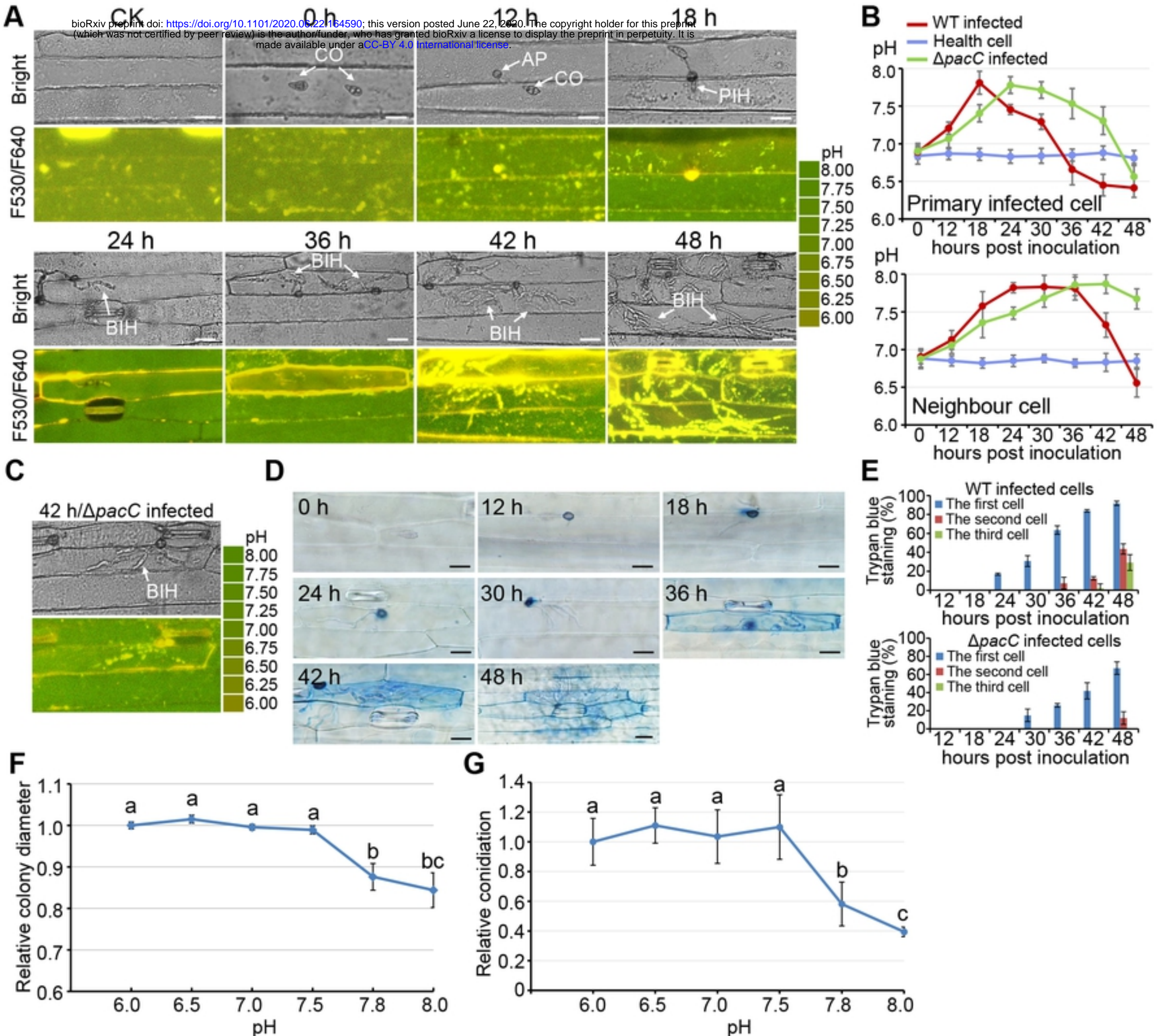


Figure 1

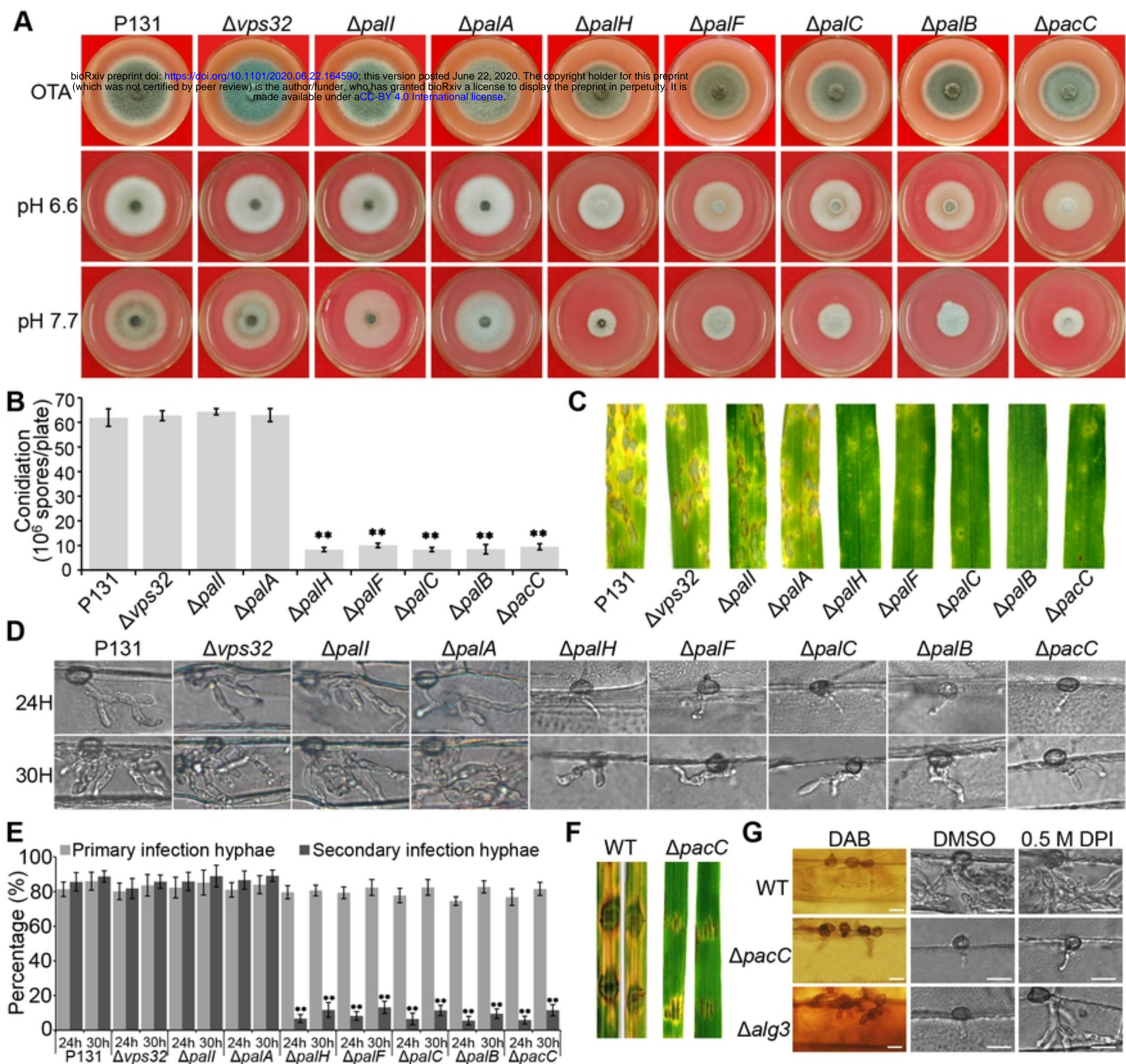
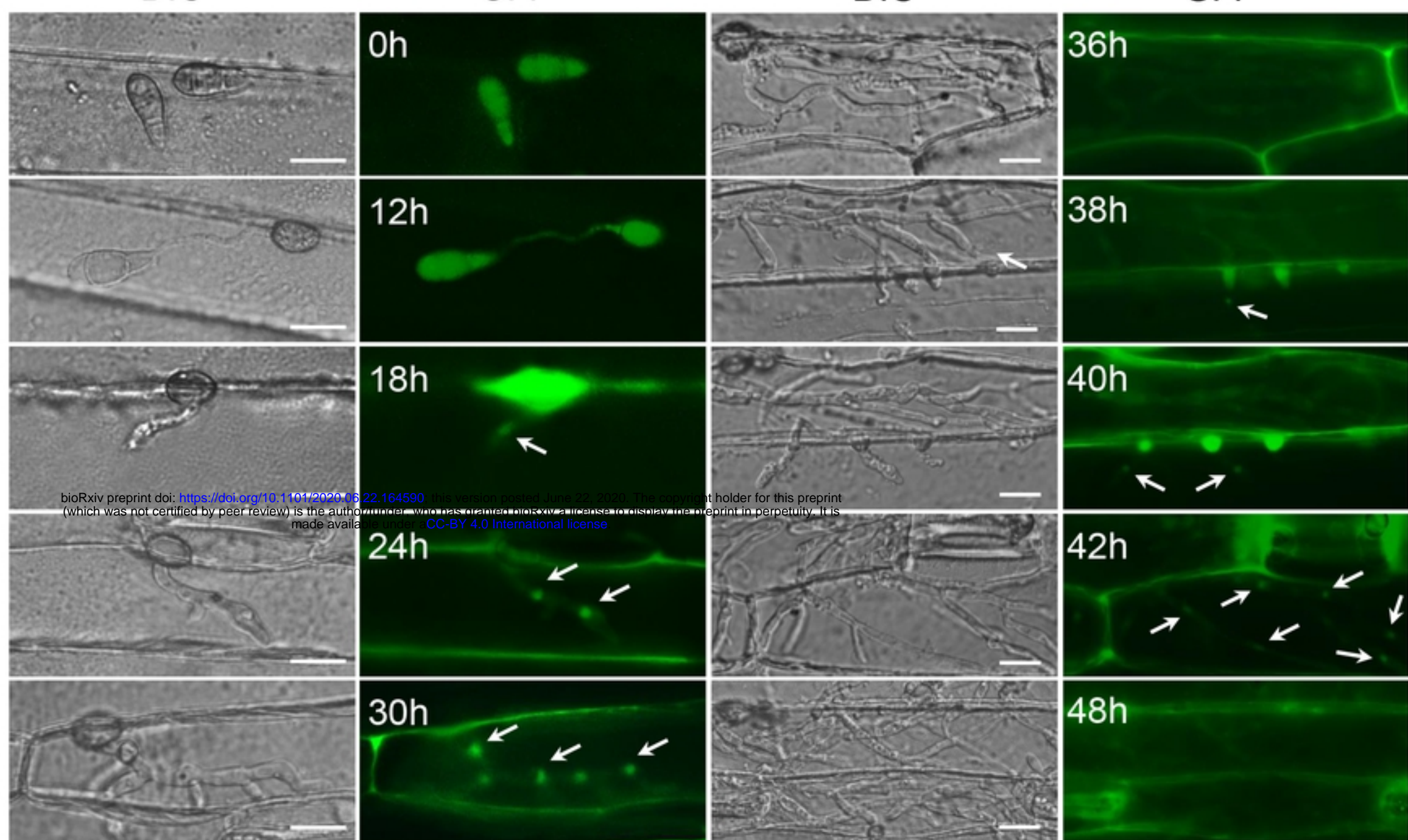
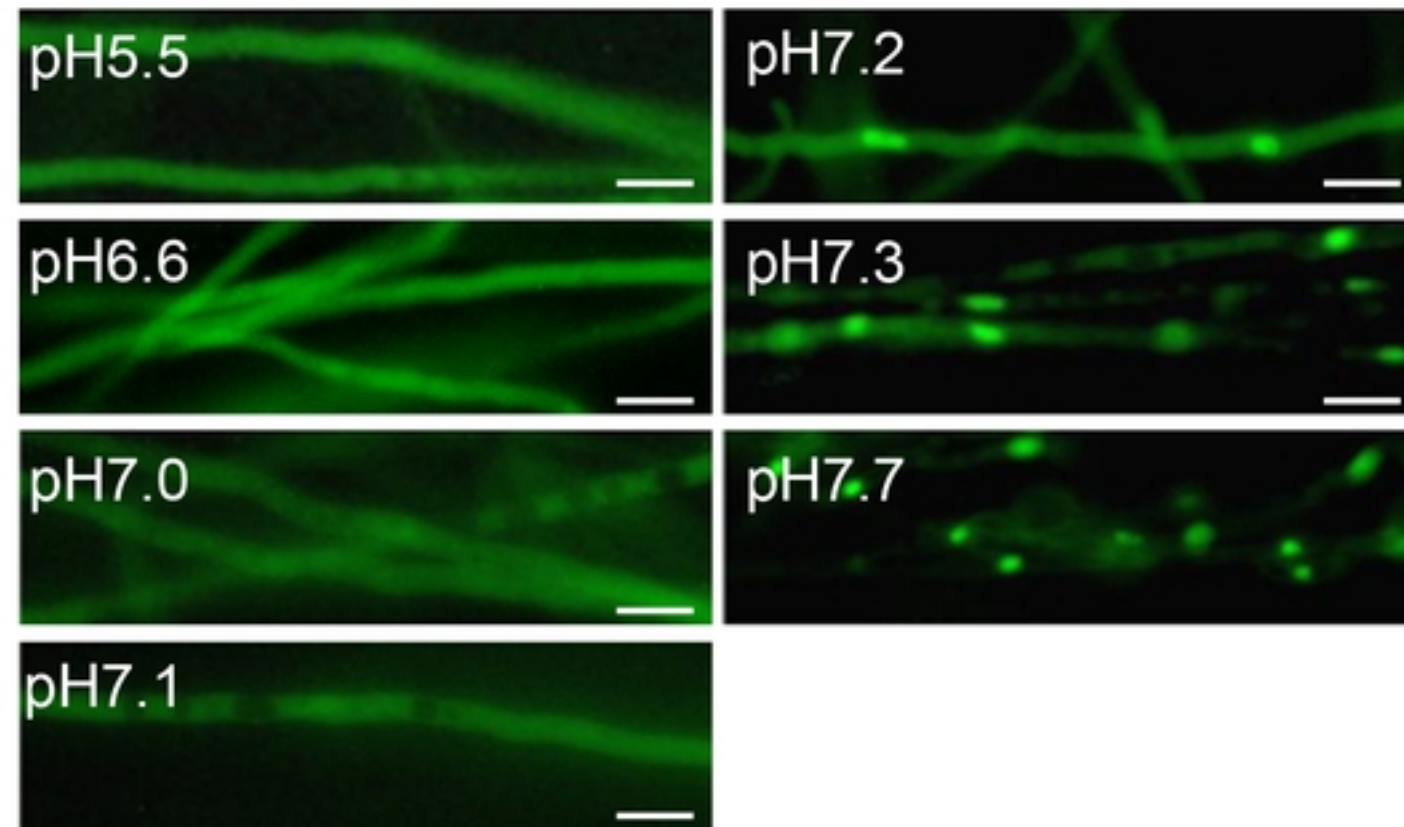
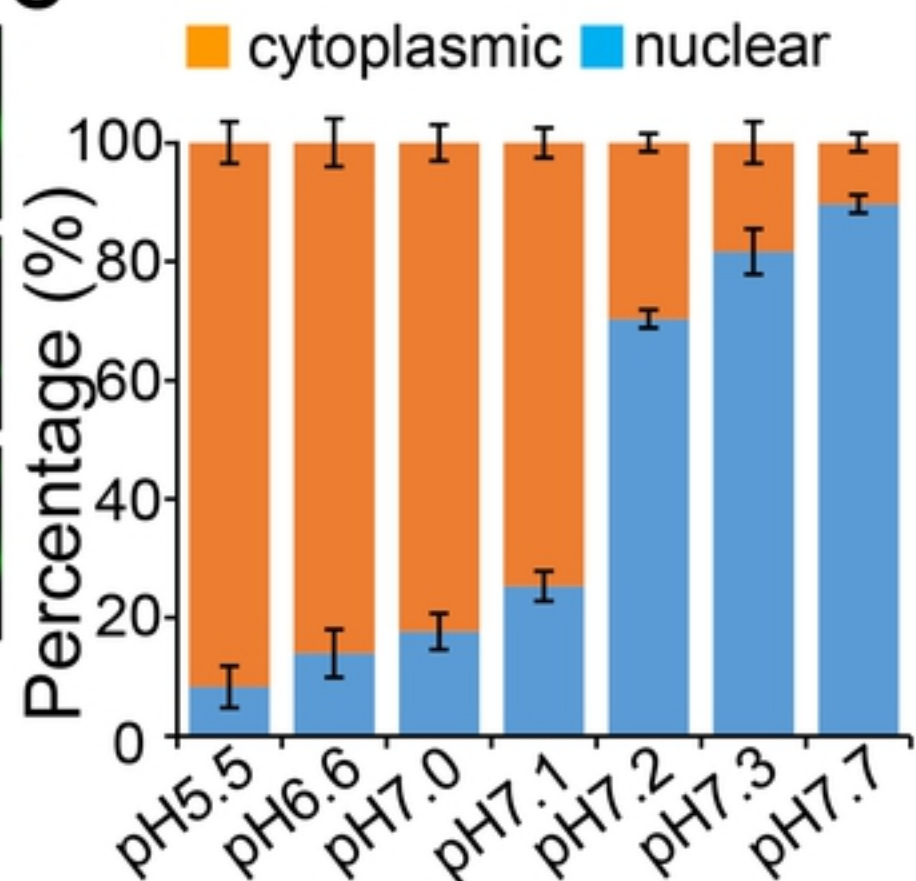
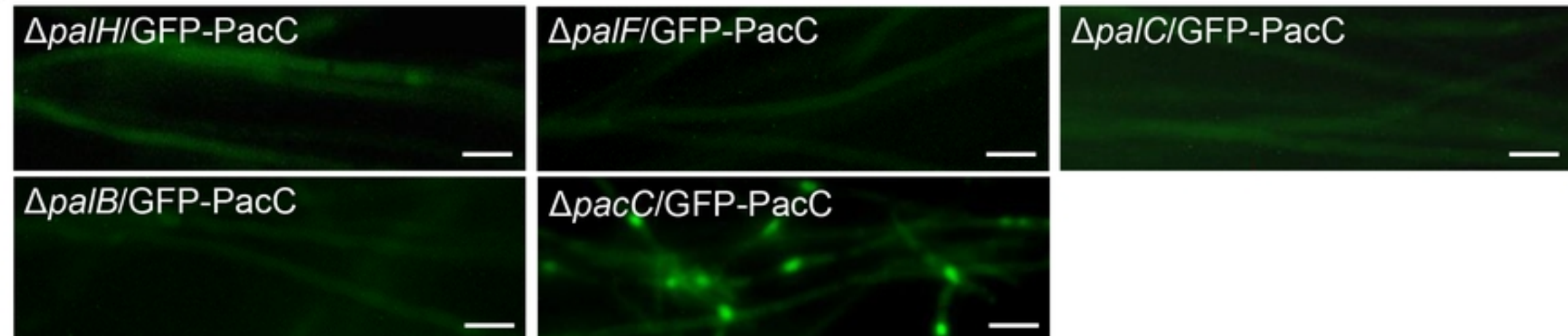


Figure 2

A**B****C****D****Figure 3**

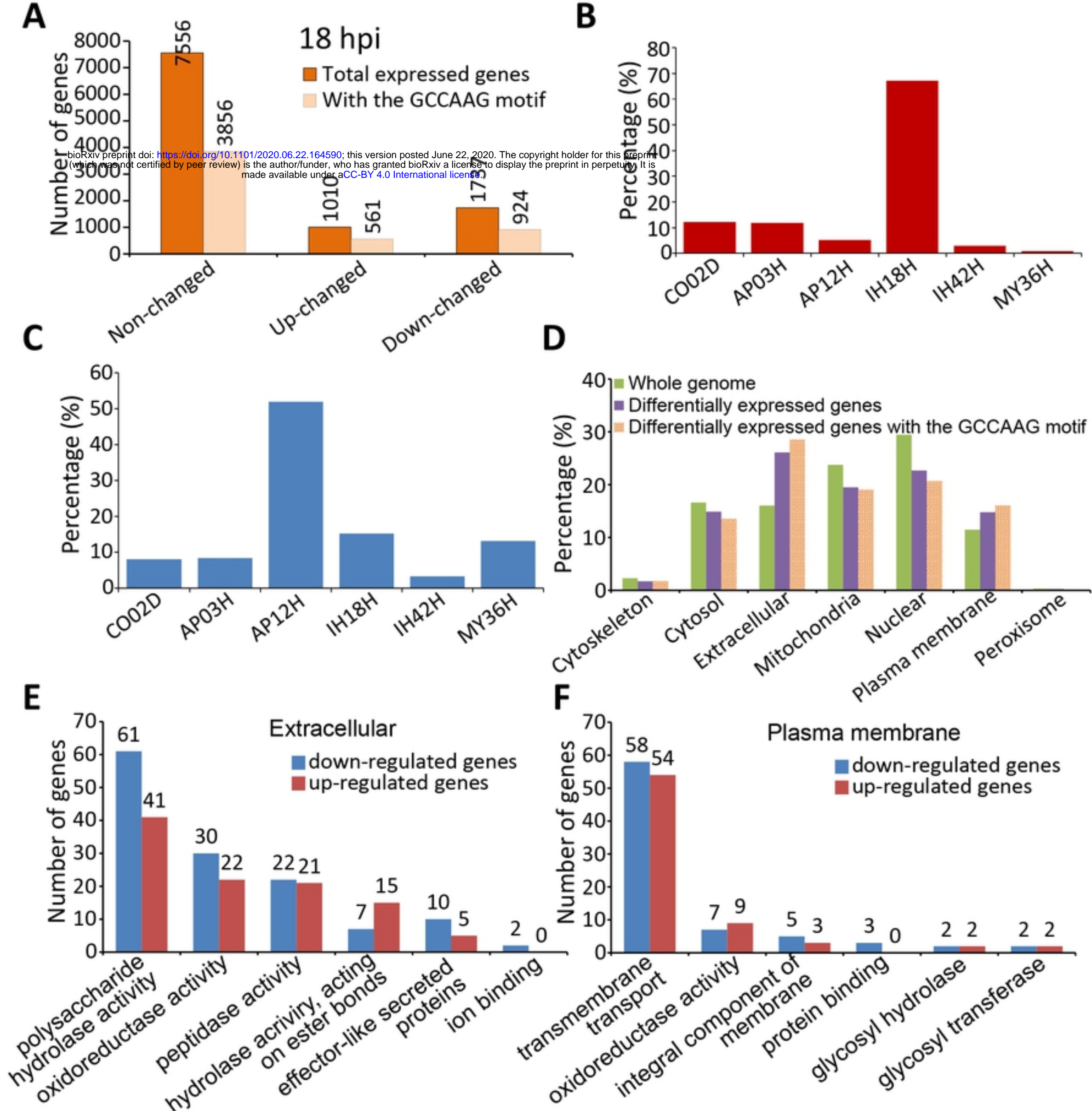


Figure 4

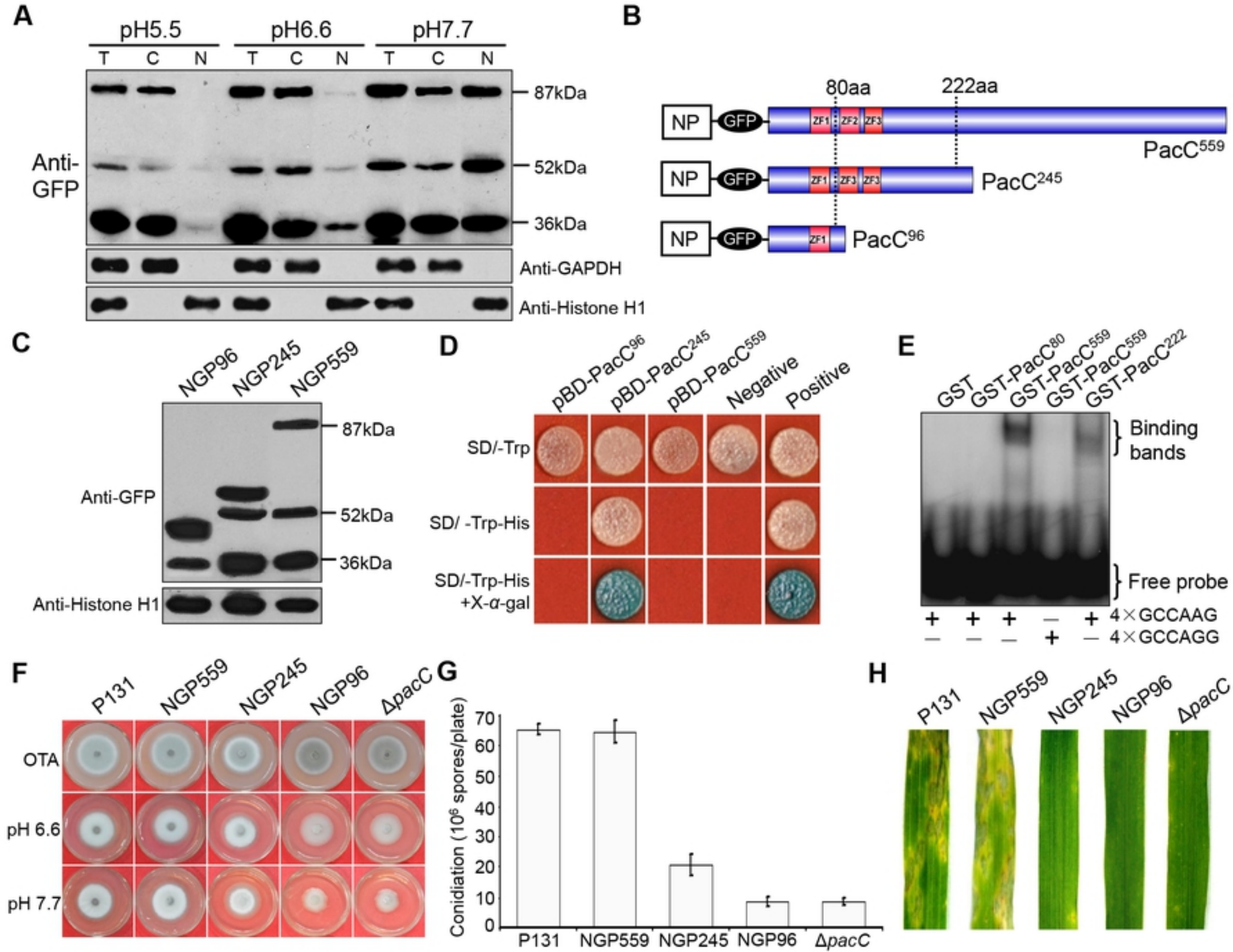


Figure 5

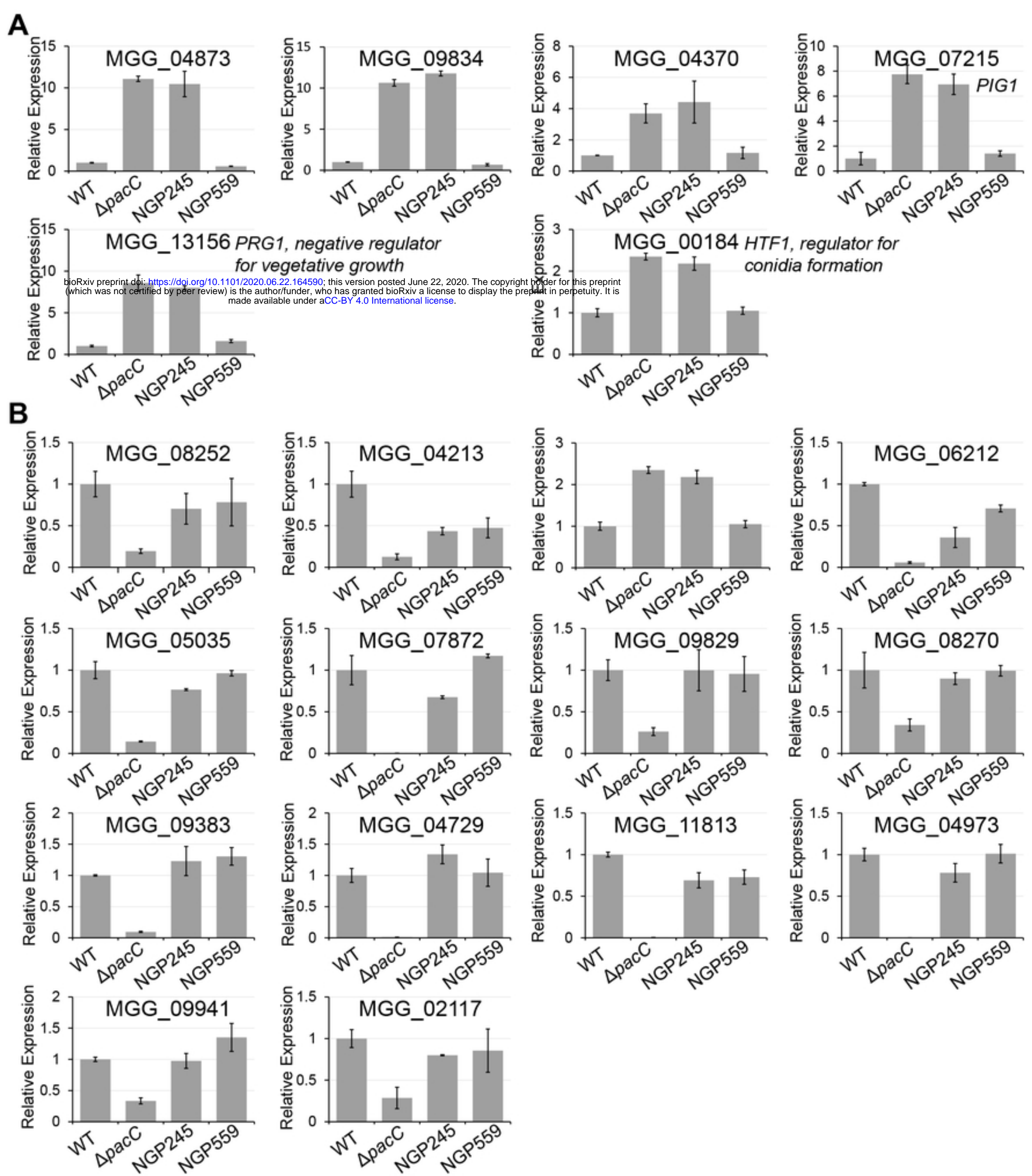


Figure 6

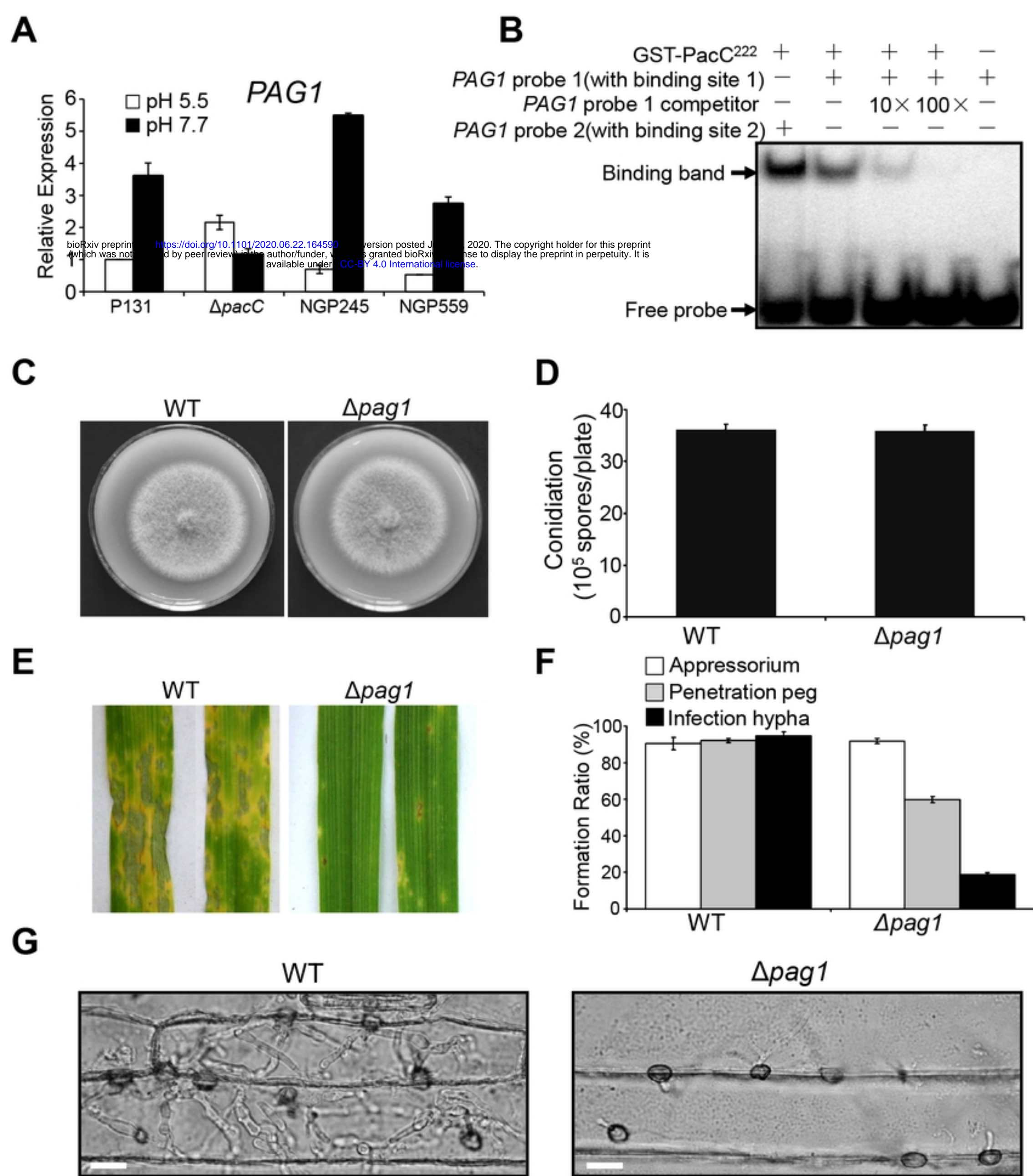
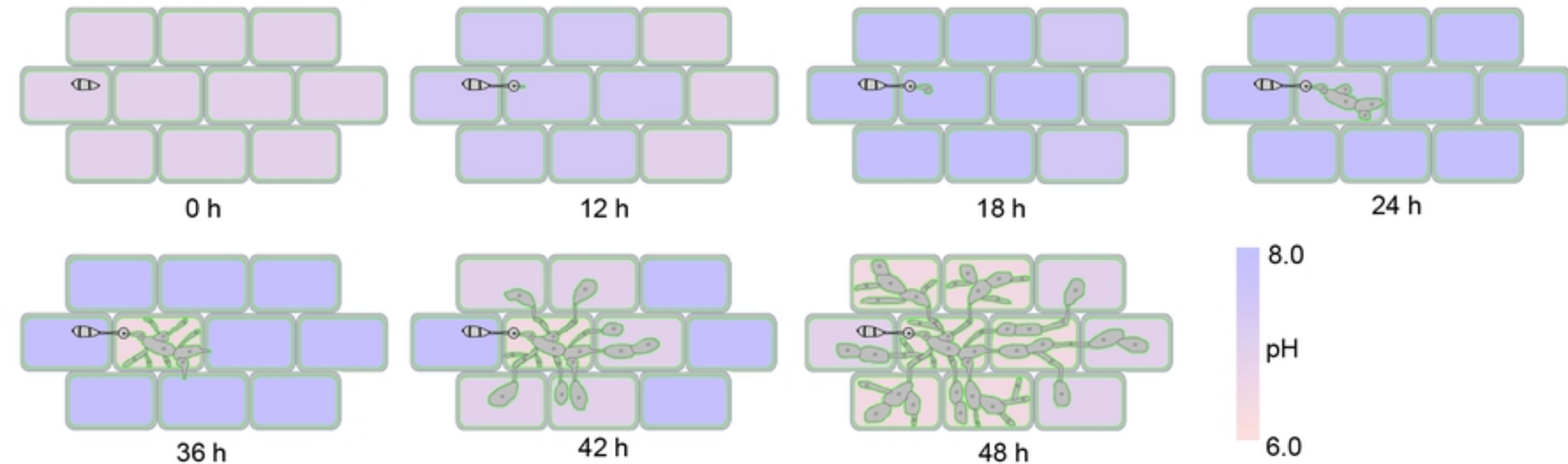
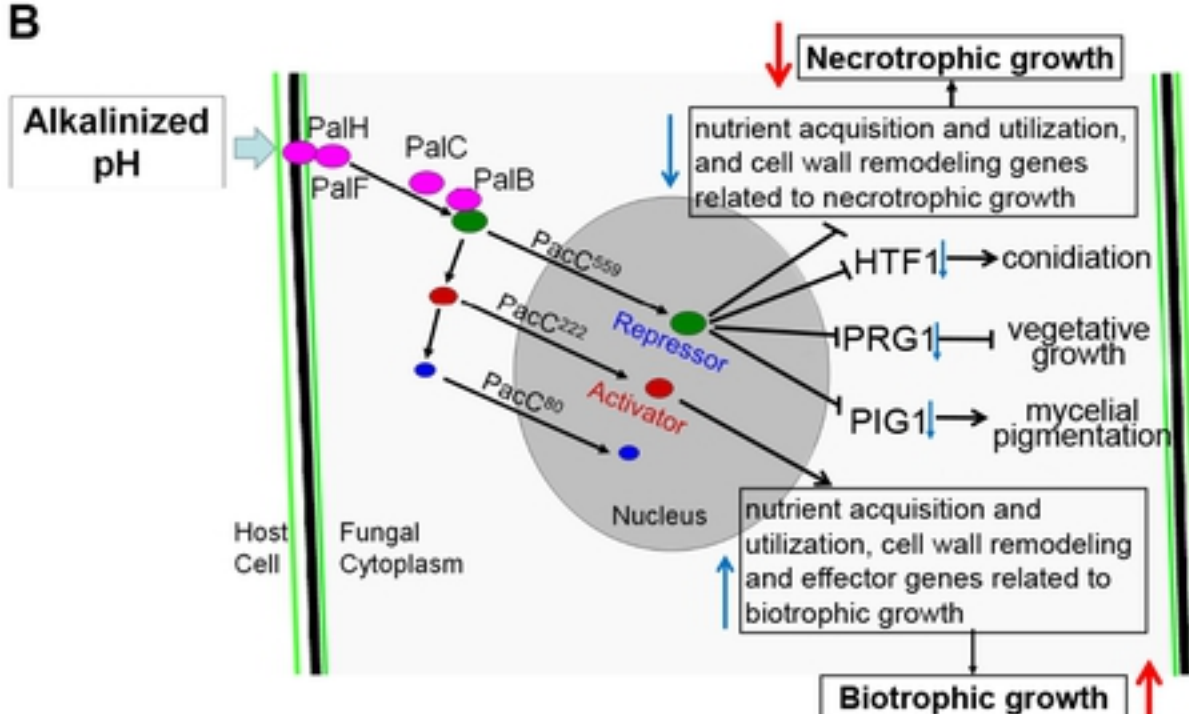


Figure 7

A



B



C

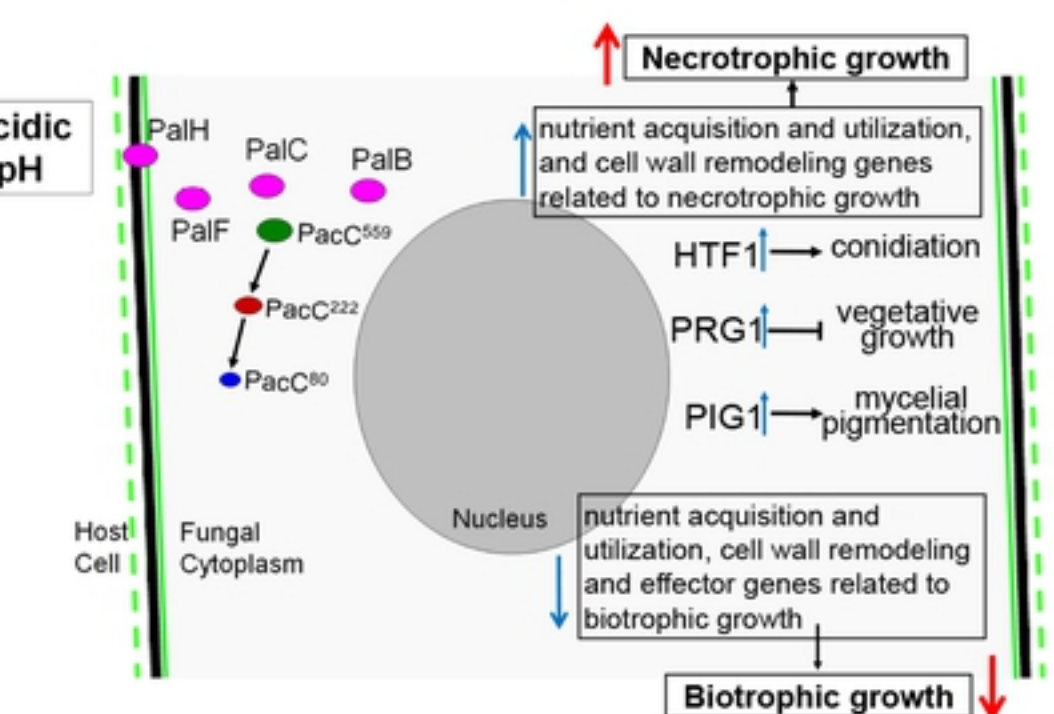


Figure 8